

1-1-2015

Metallic Encapsulation for High Temperature ($>500\text{ }^{\circ}\text{C}$) Thermal Energy Storage Applications

Abhinav Bhardwaj

University of South Florida, abhinavb@mail.usf.edu

Follow this and additional works at: <http://scholarcommons.usf.edu/etd>

 Part of the [Chemical Engineering Commons](#)

Scholar Commons Citation

Bhardwaj, Abhinav, "Metallic Encapsulation for High Temperature ($>500\text{ }^{\circ}\text{C}$) Thermal Energy Storage Applications" (2015). *Graduate Theses and Dissertations*.

<http://scholarcommons.usf.edu/etd/5843>

This Thesis is brought to you for free and open access by the Graduate School at Scholar Commons. It has been accepted for inclusion in Graduate Theses and Dissertations by an authorized administrator of Scholar Commons. For more information, please contact scholarcommons@usf.edu.

Metallic Encapsulation for High Temperature (>500 °C)
Thermal Energy Storage Applications

by

Abhinav Bhardwaj

A thesis submitted in partial fulfillment
of the requirements for the degree of
Master of Science in Chemical Engineering
Department of Chemical and Biomedical Engineering
College of Engineering
University of South Florida

Major Professor: D.Y. Goswami, Ph.D.
Elias Stefanakos, Ph.D.
John Kuhn, Ph.D.

Date of Approval:
March 23, 2015

Keywords: Renewable Energy, Corrosion, Phase Change Material,
Solar Power, Protective Coating Optimization

Copyright © 2015, Abhinav Bhardwaj

DEDICATION

I dedicate this research to my parents, Dr. Tilak Raj Bhardwaj and Kavita Bhardwaj, for their constant support and unconditional encouragement towards my educational endeavors. Mom, Dad, this would not have been possible without you.

ACKNOWLEDGMENTS

I am grateful to my major professor, Dr. D.Y. Goswami, for giving me the opportunity to work on this interesting problem. I am very appreciative for his support throughout this journey. I also appreciate all of the encouragement I received from my committee members Dr. Elias Stefanakos and Dr. John Kuhn. The research scientists of the Clean Energy Research Center (CERC) at USF, Dr. Jotshi. Dr. Dhau and Dr. Krakow, have provided valuable research insights. I thank Mr. Chuck Garretson at the CERC laboratory for sharing his knowledge of practical experimentation. I am thankful to all my colleagues at CERC for their support and the funding agency, ARPA-E, for supporting this research.

TABLE OF CONTENTS

LIST OF TABLES	iii
LIST OF FIGURES	iv
ABSTRACT	vi
CHAPTER 1: INTRODUCTION	1
1.1 Background	1
1.2 Objective of Present Work	2
CHAPTER 2: LITERATURE SURVEY	3
2.1 Concentrated Solar Power (CSP)	4
2.2 Types of Thermal Energy Storage Systems	4
2.3 Latent Heat Storage Systems	5
2.3.1 Phase Change Materials: Desirable Properties	6
2.4 Heat Transfer Enhancement Techniques	7
2.4.1 Encapsulation of PCM	7
2.5 Corrosion	9
2.6 Why High Temperature Thermal Energy?	12
CHAPTER 3: METALLIC ENCAPSULATION	14
3.1 Encapsulation Criteria	14
3.2 Operating Parameters	14
3.3 Phase Change Material	14
3.4 Encapsulation Material Selection	15
3.5 Sealing Procedure	16
3.6 Encapsulation Lining: Evaluation of Protective Coatings	17
3.7 Evaluation of Coatings	18
3.7.1 Testing in Air at 700 °C for 24-hours	19
3.7.2 Testing in Anaerobic Conditions at 700 °C for 24-hours	19
3.7.3 Preparation of Substrate	19
3.8 Results and Discussion	20
3.8.1 Testing in Air at 700 °C for 24-hours	21
3.8.2 Testing in Anaerobic Conditions at 700 °C for 24-hours	26
3.9 Optimization of Nickel Coating	28
3.10 Testing and Results	29
3.11 Encapsulation Experiment	32
3.11.1 Encapsulation Lining: Corrosion Protection	32
3.11.2 Preparation of Cylinders	33

3.11.3 Testing.....	33
3.11.4 Results and Discussion	34
3.12 Further Testing: 150 μm Nickel-Plated Cylinder	37
3.12.1 Results: After 500 Thermal Cycles.....	38
3.12.2 Results: After 1000 Thermal Cycles.....	39
3.12.3 Results: After 1700 Thermal Cycles.....	41
3.13 Chrome Coating Test	47
3.14 Aluminum Coating Test.....	50
CHAPTER 4: DISCUSSION AND CONCLUSION	52
REFERENCES	54

LIST OF TABLES

Table 1	Testing results for nickel coating thickness of 50 μm	30
Table 2	Testing results for nickel coating thickness of 100 μm	30
Table 3	Testing results for nickel coating thickness of 150 μm	31
Table 4	Weight change of samples through thermal cycling.....	48

LIST OF FIGURES

Figure 1	Sealing of cylinder containing PCM.....	17
Figure 2	Cross section of the experimental setup for anaerobic testing.....	20
Figure 3	Sealmet sample: (a) Before testing; (b) After testing: cracks observed.....	21
Figure 4	Aremco paint 634ZO (a) After air dry; (b) After curing in furnace	22
Figure 5	Bubbling observed in cured sodium silicate sample.....	22
Figure 6	Alumina adhesive sample (a) Before testing; (b) After testing: chipped.....	23
Figure 7	Alumina adhesive + silica: (a) Before testing; (b) After testing: crack	23
Figure 8	Scaling observed in case of Sealmet + sodium silicate coating.....	24
Figure 9	Electroplated nickel: (a) Before testing; (b) After testing	25
Figure 10	Alumina adhesive + sodium silicate sample failure during curing.....	25
Figure 11	Alumina adhesive + silica + sodium silicate sample failure during curing	26
Figure 12	Sealmet sample (a) Before testing; (b) After testing	26
Figure 13	Alumina adhesive sample (a) Before testing; (b) After testing	27
Figure 14	Alumina adhesive + silica sample (a) Before testing; (b) After testing.....	27
Figure 15	Electroplated nickel sample (a) Before testing; (b) After testing	28
Figure 16	Electroplated sample before testing.....	29
Figure 17	Electroplating apparatus.....	33
Figure 18	Electroplated cylinder	33
Figure 19	Cylinder electroplated in lab: After 20 cycles	34
Figure 20	Weight gain of electroplated cylinder prepared in lab.....	34

Figure 21	Weight change of ADTEC cylinder after 238 hours in air at 700 °C	35
Figure 22	ADTEC cylinder after 100 thermal cycles.....	36
Figure 23	Weight change of ADTEC cylinder after 100 thermal cycles	36
Figure 24	Thermal cycling graph (for one cycle).....	37
Figure 25	Weight change of sealed cylinder after 500 thermal cycles	38
Figure 26	Sealed cylinder after 500 cycles in aerobic conditions.....	39
Figure 27	Weight change of sealed cylinder after 1000 thermal cycles	40
Figure 28	Sealed cylinder after 1000 cycles in aerobic conditions.....	40
Figure 29	Weight change of sealed cylinder after 1700 thermal cycles	41
Figure 30	Sealed cylinder after 1700 cycles in aerobic conditions.....	42
Figure 31	Failure of electroplated 150 µm Ni cylinder between 1700 and 1800 cycles.....	42
Figure 32	DSC curve of PCM before and after undergoing 1700 thermal cycles	43
Figure 33	Electroplated Ni cylinder A (150 µm of electroplated nickel) after 60 cycles	44
Figure 34	Electroplated Ni cylinder A (150 µm of electroplated nickel) after 200 cycles and point of failure.....	44
Figure 35	SEM image depicting the thickness of nickel layer for the tested cylinders	45
Figure 36	SEM image depicting point of failure of cylinder A after 200 thermal cycles.....	45
Figure 37	Electroplated Ni cylinder B (150 µm of electroplated nickel) after 100 cycles and point of failure.....	46
Figure 38	Chrome-plated samples (a) Before testing; (b) After testing.....	47
Figure 39	Chrome-plated (75 µm) samples (a) Before testing; (b) After 200 cycles.....	48
Figure 40	Chrome plated cylinder before testing (150 µm).....	49
Figure 41	Chrome-plated cylinder (150 µm) failed after 3 thermal cycles.....	49
Figure 42	Weight change of aluminum coated carbon steel samples during testing in air at 900 °C	51

ABSTRACT

Deployment of high temperature (>500 °C) thermal energy storage in solar power plants will make solar power more cost competitive and pave the way towards a sustainable future. In this research, a unique metallic encapsulation has been presented for thermal energy storage at high temperatures, capable of operation in aerobic conditions. This goal was achieved by employing low cost materials like carbon steel. The research work presents the unique encapsulation procedure adopted, as well as various coatings evaluated and optimized for corrosion protection. Experimental testing favored the use of 150 µm of nickel on carbon steel for corrosion protection in these conditions. These metallic encapsulations survived several thermal cycles at temperatures from 580 °C to 680 °C with one encapsulation surviving for 1700 thermal cycles.

CHAPTER 1: INTRODUCTION

1.1 Background

Rising environmental concerns such as increasing concentrations of greenhouse gases and global warming have led to a greater impetus being placed on the development of renewable power generation technologies. Solar power is the front-runner amongst these technologies. However, while solar energy is a convenient renewable fuel source, it has not yet been widely implemented. This is mostly on account of the erratic availability of sunshine, both in terms of diurnal and seasonal availability. Moreover, there is variation in the demand of electricity as well. This uncertainty in the availability of sunshine coupled with the variation in consumer demand makes it difficult to bridge the gap between energy supply and demand thereby making solar power more expensive as compared to conventional power. Currently, research is focused towards technological developments that reduce this uncertainty in solar energy. Addressing this limitation would make solar energy more cost competitive against conventional fossil fuel based electricity and facilitate widespread implementation of solar power. Hence, paving the way to a sustainable future.

Thermal energy storage is one of the technologies employed to bridge the gap between electricity demand and supply. As the name suggests, it involves the storage of thermal energy during periods of abundant availability and using it during a later time of need. Hence, solar energy could be stored during a sunny day. When required, this stored thermal energy could be discharged after sunset, or on a cloudy day. Therefore, thermal energy storage will play a vital role in the deployment of solar energy towards a sustainable energy future. It helps to bridge the

gap between solar energy supply and consumer demand, hence making solar energy more dispatchable. In addition to power generation, this technology could also be employed in various manufacturing and metallurgical facilities for effective use of process heat.

1.2 Objective of Present Work

The present work is focused towards the development of metallic encapsulation for application in high temperature ($>500\text{ }^{\circ}\text{C}$) thermal energy storage applications. Steel has been used as a material for encapsulation owing to cost considerations. Since the intended application environment would be at elevated temperatures, in aerobic conditions, various coatings were evaluated to determine their corrosion protection capabilities. Furthermore, an encapsulation procedure was devised for storing thermal energy. The encapsulation was subjected to thermal cycling at $650\text{ }^{\circ}\text{C}$ for several cycles to confirm the performance of the protective coatings. The scope of the work presented comprises of:

- Encapsulation technique developed and employed for effective thermal energy storage.
- Testing and evaluation of various prospective coatings for corrosion protection.
- Optimization of thickness of protective coating employed.

The thesis is presented in four chapters. A delineation of the current work has been listed below:

- Chapter 1 presents an introduction of thermal energy storage and its importance in the development of solar energy.
- Chapter 2 reviews solar power generation technology, thermal energy storage options and metallic encapsulation. It also discusses the need for the development of high temperature thermal energy storage technology and the challenges therein.
- Chapter 3 describes experimental work conducted in this research and results obtained.
- Chapter 4 discusses the conclusion and recommendations for future work.

CHAPTER 2: LITERATURE SURVEY

Growing environmental concerns have fuelled the pace of development of solar power generation technology. Currently, solar energy is converted to electricity through either solar photovoltaic (PV) technologies or through concentrated solar power (CSP) technology.

In PV systems, sunlight is converted directly into electricity by employing solar cells that convert incident solar radiation to electricity. While this method converts solar energy directly into electricity, electricity derived from these sources is expensive on account of low efficiency of current solar cells and high cost of equipment. In case of CSP technology, solar energy is converted into thermal energy. This thermal energy is then converted into electricity through conventional thermodynamic cycle. As a result, electricity derived from CSP technology is more cost effective as compared to PV systems.

In addition to bridging the gap between supply and demand, incorporation of thermal energy storage in power plants can have additional benefits. Thermal energy storage can be used to provide ancillary services such as: load shifting, frequency regulation and, spinning reserves. Load shifting refers to moving the solar power generation from time periods of lesser demand to periods of higher electricity demand thereby providing a greater resource flexibility and profitability. Spinning reserves refers to a process employed to keep the turbine spinning/ warm in a thermal power plant. This is done in order to ramp up production quickly to meet any surge in electricity demand. These capabilities are two of a larger set of properties often referred to as dispatchability [1]–[3]. These services also reduce dependence of the power grid on peaker

plants that burn fossil fuels to generate electricity. These peaker plants rely on petroleum derived fuels in order to meet the grid requirements during periods of high demand.

This following discussion would focus on CSP technology as well as thermal energy storage using phase change materials (PCMs).

2.1 Concentrated Solar Power (CSP)

In case of CSP technologies, incident solar radiation is converted to thermal energy by employing solar thermal collectors. The operating principle of these collectors is based on the fact that incident radiation striking an object is partly absorbed thus leading to a rise in its temperature [4]. The efficiency of these concentrators is dependent on two factors: (i) absorption efficiency, as well as, (ii) how the energy is removed from the collector for useful purposes. Solar thermal collectors vary from unglazed flat plate type collectors operating at 5-10 °C above ambient temperatures as well as high temperature collectors. Central receiver concentrating collectors are capable of operating at temperatures of 1000 °C [4].

Concentrators focus the sunlight onto absorbers that convert photons into heat. This heat energy is transferred to a working fluid. This working fluid is used to drive a turbine and generate electricity. CSP technology is closer to more prevalent conventional power generation technologies that rely on conversion of heat energy to electricity.

2.2 Types of Thermal Energy Storage Systems

Thermal energy can be stored through three methods: (i) Sensible heat storage, (ii) Latent heat storage, and (iii) Thermochemical storage. Energy content of a material rises with increase in temperature. In case of sensible heat storage systems, the energy is absorbed or released by heating or cooling the thermal energy storage media. It is important to note here that the storage media does not undergo any phase change. In case of latent heat storage systems, the energy is

stored or released while the material undergoes a phase change (e.g. solid to liquid). These energy storage materials are referred to as phase change materials (PCMs). These systems allow for higher energy densities than sensible heat storage systems. Thermochemical heat storage systems rely on chemical energy between bonds. The energy is stored or released during reversible endothermic reactions. Currently, prevalent thermal energy storage systems are the sensible and latent heat storage systems.

2.3 Latent Heat Storage Systems

Thermal energy can be stored approximately isothermally in these systems. The phase transitions involved are mostly solid to liquid. Alternately, liquid to vapor transitions could be employed, however, there would be a significant volume change in these cases thereby requiring significant investment on larger storage tanks. These storage systems possess high energy density thereby reducing energy storage costs [5].

Study of latent heat thermal energy storage systems requires understanding of PCMs and the heat exchange processes occurring during melting and solidification of the PCM inside the containment. A PCM should have good thermophysical properties. During the charging process, the PCM would absorb the solar energy and undergo phase change from solid to liquid. When there is requirement of energy to meet peak load demand, the PCM should undergo phase change from liquid to solid during the discharging process. While the PCM should have good thermophysical properties to absorb and release heat, it should also possess good thermal conductivity in order to undergo these transitions at a decent rate. Hence, the process of energy storage and utilization would be effective and efficient. Various steps involved in the development of latent heat storage systems have been presented by Abhat et al. [6].

2.3.1 Phase Change Materials: Desirable Properties

Abhat et al. [6] discussed some of the desired properties of ideal PCMs. Based on various thermodynamic, kinetic, chemical and economic considerations:

- The PCM should possess melting point in the temperature range of the intended application
- The PCM should have a high latent heat and high density in order to store maximum energy in lesser amount of PCM
- The PCM should exhibit good thermal conductivity in order to exhibit fast charging and discharging rates
- The PCM should exhibit small volume changes during phase transition
- The PCM should be chemically stable in the desired application
- The PCM should have no or minimal super cooling
- The PCM should be non-corrosive, non-toxic, non-flammable, non-poisonous, and, non-explosive
- The PCM should be readily available, abundant and inexpensive

Various other studies by Lane [7], Dincer and Rosin [8], and Zalba et al. [9] have presented a comprehensive analysis of PCMs, their classifications, and characteristics. Most PCMs that meet the criteria of economic, chemical and and kinetic considerations suffer from low thermal conductivity of approximately 0.5 W/mK [10]. This leads to poor heat transfer between the heat transfer fluid and the storage media. For the current study, chloride based salts (NaCl-KCl) were used as PCMs due to their attractive thermophysical properties and low cost. The following section presents some of the heat transfer enhancement techniques employed by various researchers.

2.4 Heat Transfer Enhancement Techniques

To address the aforementioned problem of low thermal conductivity of PCMs, various researchers have proposed numerous techniques to enhance effective thermal conductivity.

Enhancement of thermal conductivity by employing finned tubes in different configurations was presented by various researchers [11]–[18]. Numerical and experimental results for vertical cylinders enhanced with fins were provided by Ismail et al. [19]. Choi et al. [20] presented the results for finned and unfinned tube units employing $\text{MgCl}_2 \cdot 6\text{H}_2\text{O}$ as PCM. Unlike PCMs, metals possess high thermal conductivity. Hence, several researchers have explored the incorporation of metal matrices in PCMs to enhance thermal conductivity of the thermal energy storage system [21], [22]. Trelles et al. [21] employed aluminum matrices to provide cooling for a vaccine refrigerator. High conductivity materials dispersed in PCMs were studied by Eman-Bellah et al. [23]. Their study employed the usage of aluminum powder in paraffin wax for conductivity enhancement. Furthermore, shell and tube configurations [24], [25] for latent heat thermal energy storage systems have also been studied. Agyenim et al. [24] presented numerical and experimental results for a horizontal shell and tube thermal energy storage system. Various researchers have studied cascade systems [26]–[28] that employ a range of PCMs with different melting points in order to improve the performance of the system. In addition, encapsulation of PCM has also been used to improve the thermal conductivity of the system [29], [30].

2.4.1 Encapsulation of PCM

Encapsulation of PCM is a vital criterion for employing thermal energy storage systems. In addition to providing containment of the energy storage media, encapsulation provides the benefit of improving the thermal conductivity of the storage system. Rate of charging and

discharging processes in thermal energy storage systems are dependent on area available for heat transfer. Hence, the encapsulation acts like a thermal energy cell. Encapsulation of PCM leads to an increase in surface area available for heat transfer thereby improving the thermal conductivity of the system. A review regarding thermal energy storage employing PCM capsules was presented by Regin et al. [31]. Some of the important requirements regarding PCM encapsulation are as follows:

- It must strengthen corrosion resistance and thermal stability in the operating conditions
- Effective containment of the PCM for a satisfactory time period at elevated temperatures
- Provide sufficient surface for heat transfer [31], provide structural stability and easy handling [31]

Encapsulation can be classified into three types depending on the size of encapsulation [32]:

- 1) Macroencapsulation (above 1 mm)
- 2) Microencapsulation (0-1000 μm)
- 3) Nanoencapsulation (0-1000 nm)

Macroencapsulation is a common technique applied to encapsulate PCM. Salunke et al. [32] presented a list of various manufacturers of macroencapsulated PCMs in various shapes. Furthermore, while most applications used plastic materials as shell casing, some high temperature applications also employed aluminum for shell construction.

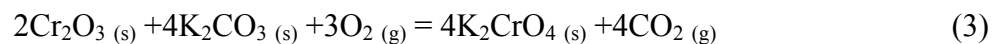
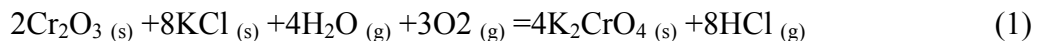
Microencapsulation refers to encapsulation sizes of less than 1mm. Higher surface area to volume ratio allowed by employing this strategy yield higher heat transfer areas than macroencapsulation [33], [30]. Hawlader et al. [30] presented a study on the preparation and characterization of paraffin wax employing SEM and DSC. Griffiths et al. [29] employed microencapsulation of PCMs for chilled ceiling panels.

Nanoencapsulation refers to encapsulation diameters up to 1000 nm. Fang et al. [34] prepared nanocapsules employing in situ polymerization. While N-Tetradecane was used as the PCM, urea and formaldehyde were used for the shell material. Another publication [35] employed n-octadecane as the PCM and polystyrene as the encapsulation material.

As presented in this section, there are different types of encapsulation depending on size. High temperature applications (600 °C) of thermal energy storage require metal as material of encapsulation since polymers would degrade at these temperatures. Since this study was focused on high temperature thermal energy storage using inorganic chloride salts, hence, further discussion would focus on metallic encapsulation of PCMs and the challenges faced therein. One of the major challenges associated with metals employed with chloride salts like NaCl and high temperatures is corrosion. The following section would present literature survey of studies regarding corrosion in the aforementioned conditions.

2.5 Corrosion

Corrosion of metals at high temperatures is accelerated in the presence of salt [36]. Various explanations have been proposed for this behavior. This has been attributed to the dissolution of protective layers of Al₂O₃ and Cr₂O₃ by molten salt [37]. Moreover, production of HCl and SO₂ by dissolution of the molten salt have also been mentioned as additional factors for this accelerated process [37]. The reaction between the protective chromium oxide layer and the alkali chloride was presented by Lehmusto et al. [38] as follows:



Hence, the presence of moisture and oxygen facilitates the reaction of protective chromium oxide layer thereby aggravating corrosion. This presented a significant challenge to the metallic encapsulation of inorganic salts for applications at high temperatures.

While expensive materials like nickel and Hastelloys have been studied by various researchers for similar applications [38], they are not cost effective solutions for the proposed study. Several studies have analyzed the problem of corrosion of metals at elevated temperatures in salts. Zhou et al. [39] studied the effects of chromium, nickel and copper on the corrosion behavior of low carbon steel in chloride environments. They proposed that the addition of nickel and chromium led to the formation of dense, compact rust layers on top of the substrate thereby protecting it from further oxidation. Hiramatsu et al. [36] studied the effects of various alloying elements on sodium chloride induced corrosion in a temperature range of 450 °C to 750 °C. Austenitic steel were found to exhibit better resistance than ferritic steels. Furthermore, nickel was found to be effective in corrosion protection. Coyle et al. [40] performed testing on alloys in molten salts at 900 °C. Characterization studies of corrosion using SEM/EDXA analysis were conducted by Lehmusto et al. [41] to study the effect of solid KCl on superheater steels at elevated temperatures. Nickel-based alloy 625 type steel exhibited superior corrosion resistance as compared to ferritic 10CrMo type steel. In case of the alloy 625 type steel, the thick oxide layer was predominantly nickel oxide. The study presented the following mechanism for the reaction and subsequent degradation of the protective chromium oxide layer.

The costs of nickel alloys are approximately 4 times greater than the cost of stainless steel alloys [2]. Hence, the successful encapsulation would be a synergistic combination of the cost-effectiveness of steel and the corrosion resistance of nickel alloys. In addition, Evans et al. [42] presented a comprehensive analysis of various Fe-Cr-Ni alloys. Diffusion of chromium ions

in the Cr_2O_3 scale was found to be the rate controlling step at elevated temperatures of 700 °C. Mohanty et al. [43] studied the role of chlorides in hot corrosion of high alloy stainless steels. As per the study, thermal cycling was an integral part of the degradation process.

Various researchers have also evaluated corrosion protection using protective coatings in aforementioned conditions. Performance of yttria-stabilized zirconia coating on 316L SS as compared and to uncoated 316L SS studied by Shankar et al. [44]. The testing was carried out at elevated temperatures of 600 °C in molten LiCl-KCl salt, and the coating was found to be instrumental in providing improved corrosion resistance. The presence of oxygen and/ or moisture was found to accelerate corrosion process [44]. Experimental studies of boiler steels and protective coatings were conducted by Uusitalo et al. [45] at high temperatures. The study evaluated high velocity oxy-fuel (HVOF) coatings, laser cladding, and diffusion chromized steel. Three types of boiler steels were also analyzed. Nickel-based high chromium coatings were found to exhibit satisfactory results during testing.

Corrosion could be prevented by the use of expensive alloys, employing protective coating or by employing an atmosphere that does not have oxygen or moisture to facilitate oxidation of the sample. In order to maintain cost effectiveness, an inert atmosphere could not be deployed at the scale of the intended application. The material to be used for heat transfer would have to be air. Hence other options were evaluated for corrosion protection. Currently, various efforts are underway to improve the corrosion resistance technology such as development of new alloys and protective coatings. Other corrosion resistance techniques include shot peening, cladding and internal insulation approach [2]. In shot peening, the surface of the material is modified through impingement. This results in changing the grain size and the structure of the

alloy at the surface. Smaller grain size provides a larger surface area for formation of passivating layers thereby improving corrosion resistance [46].

Another technique employed for surface protection is Cladding. It involves bonding thin layers to a substrate through roll welding, explosive welding or laser application, hence, providing protection. The internal insulation approach is an economical option to provide corrosion resistance. It employs thermally insulating refractory bricks as internal liner to the storage tank. This approach has been employed in coal gasification industries [47].

2.6 Why High Temperature Thermal Energy?

Exergy is defined as the maximum theoretical useful work as the system is brought into complete thermodynamic equilibrium with the environment [48].

In a CSP based solar power plant, the thermal energy storage unit is paired up with the power block that converts thermal energy to electricity. This conversion process is bound by the Carnot efficiency and hence, it is imperative to draw out the thermal energy at the maximum possible temperature to pair it with the power block. If the temperature at which this energy was extracted was much lesser than the operation temperature of the power block, it results in a loss of thermal energy available for conversion to electricity. This would lead to reduced exergetic efficiency. In case of a TES system, exergetic efficiency can be defined as the ratio of Gibbs free energy change during discharging, $\Delta G_{\text{discharging}}$, to the Gibbs free energy change during charging, $\Delta G_{\text{charging}}$ [2]. This can be mathematically expressed as:

$$\eta = \frac{|\Delta G_{\text{discharging}}|}{|\Delta G_{\text{charging}}|} = \frac{|(\Delta H - T_{\infty} \Delta S)_{\text{discharging}}|}{|(\Delta H - T_{\infty} \Delta S)_{\text{charging}}|} \quad (4)$$

where T_{∞} represents ambient temperature and ΔH and Δs represent change in enthalpy and entropy, respectively. Furthermore, since this TES system would be paired up with the power block, Stekli et al. approximated the following expression for exergetic efficiency:

$$\eta = \frac{Q_{out}}{Q_{in}} \times \frac{W_{out}}{W_{in}} \approx \frac{Q_{out} \cdot (1 - \frac{T_{\infty}}{T_{ht}})}{Q_{in} \cdot (1 - \frac{T_{\infty}}{T_{sf}})} \quad (5)$$

where, Q_{out} is the total energy transferred from the TES system to the heat transfer fluid during discharging and Q_{in} refers to the total energy transferred from the heat transfer fluid to the TES system during charging. T_{ht} represents the temperature of the working fluid at the turbine inlet (in Kelvin) and T_{sf} represents the temperature of the heat transfer fluid at the outlet of the solar field (in Kelvin).

It is evident from equation (5) that operating at elevated temperatures can increase the exergetic efficiency of the CSP power plant. However, there are certain challenges associated with operating at higher temperatures like material selection, corrosion, loss of mechanical strength to name a few.

Currently, of the five solar power plants under construction in the U.S., only two would incorporate thermal energy storage. These are the 250 MW Solana Generating Station (Abengoa Solar, Inc.) and the 110 MW Crescent Dunes Solar Energy Project (SolarReserve, LLC). The absence of thermal energy storage is largely due to additional capital cost of incorporating thermal energy storage capabilities.

To address the current high cost of solar derived electricity, the U.S. Department of Energy launched the SunShot Initiative in 2011. This was a national endeavor to make unsubsidized solar energy cost competitive by 2020. For CSP technology the goal is to bring the cost of unsubsidized levelized cost of electricity to \$0.06 /kWh by 2020 [49].

CHAPTER 3: METALLIC ENCAPSULATION

3.1 Encapsulation Criteria

The development of the encapsulation is an integral part of applying the thermal energy storage concept. The encapsulation development process relies on careful evaluation of operational requirements, selection of prospective PCMs, materials of encapsulation, and the sealing process employed. Furthermore, in-depth experimentation to determine suitable options and their optimization is also required. For the current study, cost considerations guided most of the material selection process. This chapter discusses the results of experimentation carried out to determine the above-mentioned criteria.

3.2 Operating Parameters

The thermal energy storage criteria required the ability to store thermal energy at elevated temperatures of 600 °C. Moreover, this thermal energy storage capability had to employ air as the heat transfer fluid since steam produces very high pressures at elevated temperatures, thereby, requiring significant investment to reinforce structures. The encapsulation material had to be robust to meet these criteria in a cost effective manner.

3.3 Phase Change Material

The phase change material selected for this study was NaCl-KCl eutectic. This eutectic is a 50 mol % mixture of the two inexpensive components. It has a melting point of 656.7 °C and a latent heat of 360 J/g. Besides being cost effective, the material is non-toxic and is infrared (IR) transparent. At high temperatures, radiation becomes an important contributor of heat transfer and hence the use of IR-absorptive additives could be justified for such PCMs.

3.4 Encapsulation Material Selection

Material selection is a critical part of development of high temperature thermal encapsulation. The encapsulation material had to meet the operating requirements of the application in a cost effective manner. It had to be robust and resist corrosion under aerobic conditions at elevated temperatures.

Additionally, this material must be inexpensive to meet the ARPA-E project goal of thermal energy of \$15 /kWh thermal. This is a tall order to meet for any individual material. Therefore, it was best estimated to use a combination of materials that would successfully hold the PCM at high temperatures without reacting with it. Moreover, a protective coating would prevent corrosion of the encapsulation material and hence resist any degradation of the encapsulation.

Carbon steel, while affordable, does not fare well in aerobic conditions at elevated temperatures. Alternately, corrosion resistant nickel based alloys are expensive. Hence, the optimum solution required the cost effectiveness of the carbon steel and the corrosion resistance of nickel based alloys.

Corrosion relies on an oxidizing atmosphere to occur. The exterior of the encapsulation would be subjected to the heat transfer fluid (i.e. air) Hence the exterior of the encapsulation required a corrosion resistant protective coating. The interior of the encapsulation would be in contact with PCM at elevated temperatures. This would be a highly corrosive environment under aerobic conditions. However, in the absence of oxygen, the interior of the encapsulation might not require any protection. Hence, a method was devised to seal the encapsulation under inert conditions in order to ensure anaerobic conditions in the interior of the encapsulation. This method of sealing the encapsulation is discussed in the next section.

In order to achieve an optimal solution, various coatings were used with carbon steel as substrate. These protective coatings were tested in laboratory scale experiments under aerobic and anaerobic conditions for a specific time period for preliminary results. Based on these results, shortlisted coatings were tested for extended durations. The testing was performed in both aerobic and anaerobic conditions so as to observe the performance of various coatings and to devise a successful encapsulation of thermal energy for high temperature applications.

3.5 Sealing Procedure

Cost effective solution approach dictated the use of carbon steel as the encapsulation material. However, it presented problems associated with corrosion at elevated temperatures. Moreover, coupled with salt as the corrosive environment and air as the oxidizing media further complicated the process. Analysis of this complication led to exploration of ways to simplify the problem.

The solution came by designing an ingenious encapsulation sealing process. This process involved sealing the encapsulation through welding in an inert atmosphere. The inert atmosphere would ensure absence of oxygen and hence, would reduce chances of corrosion. The encapsulation containing the PCM was heated in a tube furnace in order to melt the PCM. It was placed in a mullite tube flushed with inert gas. This ensured that the exterior of the encapsulation was heated in the absence of air. Hence, reducing chances of corrosion at the exterior of the encapsulation. The interior of the encapsulation was also flushed with inert gas so as to ensure absence of oxygen. Once the PCM was melted, welding a cap on top of the encapsulation sealed the capsule. This method simplified the complicated corrosion protection problem. With the interior of the encapsulation possessing an anaerobic atmosphere to avoid corrosion, it was now required to identify a coating that would protect the exterior steel at elevated temperatures in air.

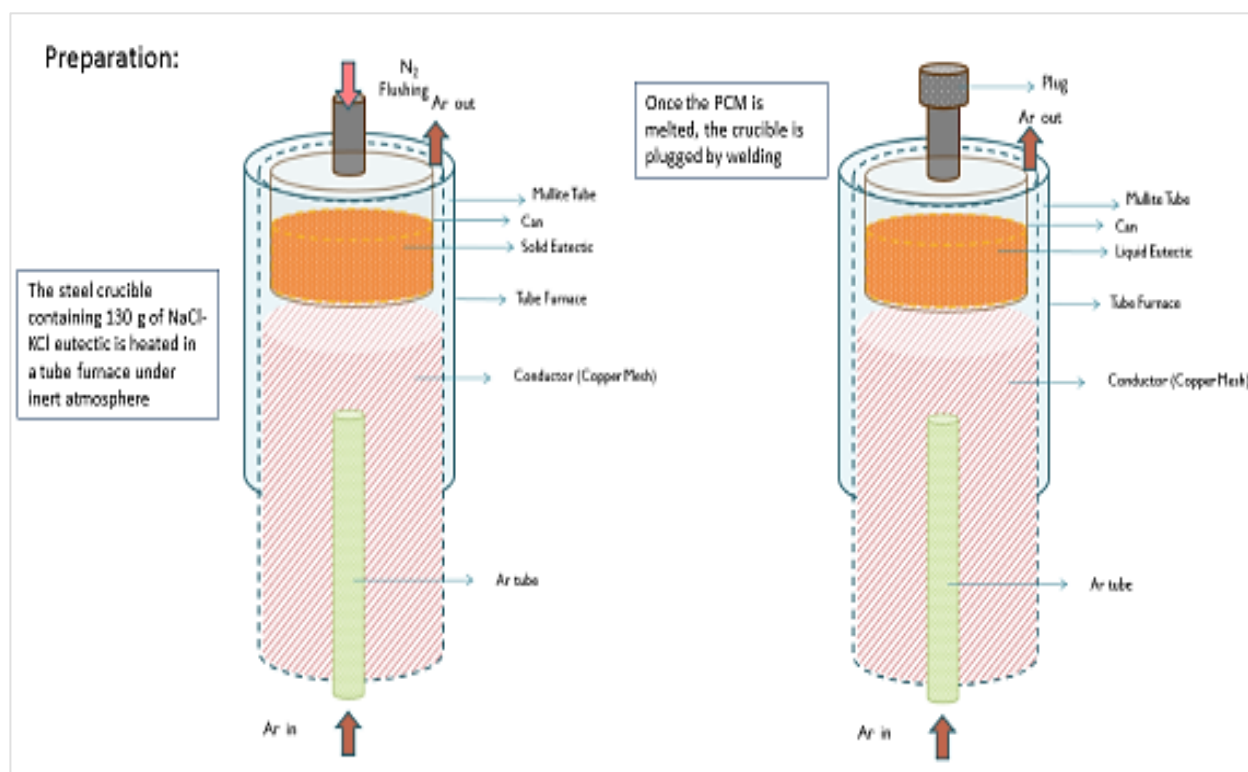


Figure 1 Sealing of cylinder containing PCM

3.6 Encapsulation Lining: Evaluation of Protective Coatings

For the purpose of corrosion protection, several coatings were shortlisted in order to determine their efficacy in protecting steel at elevated temperatures of 700 °C. For this purpose, materials selected were ceramic-based coatings and metal alloy coatings. While ceramic-based coatings have had applications in high temperature conditions, their ability to have a uniform non-porous coating on the metallic substrate would prove to be a challenge. Moreover owing to the different coefficients of expansion, both the material and the substrate would have different expansions during thermal cycling thereby leading to possible spalling of the coating. These ceramic coatings were Alumina or silica based. Moreover, high temperature metal coatings (such as nickel) were also used to determine their performance. The preliminary results obtained in this study were further used in order to determine the optimum thickness of coating required.

3.7 Evaluation of Coatings

Based on the previously discussed criteria, following coatings were evaluated:

- 1) Sealmet
- 2) Aremco: Pyro-paint 634-ZO
- 3) Sodium silicate
- 4) Alumina adhesive
- 5) Alumina adhesive + silica
- 6) Sealmet + sodium silicate
- 7) Aremco: Pyro-paint 634-ZO + sodium silicate
- 8) Electroplated nickel
- 9) Alumina adhesive + sodium silicate
- 10) Alumina adhesive + silica + sodium silicate

The selection of these coatings was done in order to derive the best of three properties namely: adhesion, coverage and porosity to air. The ideal coating would have perfect adhesion to the substrate at elevated temperatures and would cover the entire surface during the curing process thereby protecting the substrate. Furthermore, it was important that the coating be impervious to air in order to protect the underlying steel surface from oxidation. Additives like sodium silicate and silica were also used alongside these coatings to improve their performance by improving their adhesion, coverage and impervious characteristics.

For the determination of corrosion protection capabilities, testing was pursued for the following two conditions i.e. aerobic, as well as anaerobic environments. While the application warranted the use of protective coating for elevated temperatures in aerobic conditions, anaerobic testing was also pursued in order to meet the criteria of the encapsulation sealing

process. This section would present the details of the testing procedure as well as the results obtained. These results were used for further optimization studies to determine coating thickness. The duration for most of these preliminary tests was 24 hours. During the course of testing, the samples were periodically weighed and photographed in order to document their progress. The results were based on two criteria: (i) appearance (cracking and scaling), and. (ii) weights of the samples on conclusion of the testing.

3.7.1 Testing in Air at 700 °C for 24-hours

In this case, the coatings were tested at a temperature of 700 °C in air for 24 hours in the absence of phase change material. This was done to emulate the exterior surface of encapsulation using air as HTF. In a practical application, the exterior of the encapsulated thermal energy cell would be subjected to air at these temperatures.

3.7.2 Testing in Anaerobic Conditions at 700 °C for 24-hours

To mimic the interior of the cylinder, testing was done in the absence of air at 700 °C for 24 hours in the presence of a known amount of phase change material (approximately 28 g).

For anaerobic testing, samples were placed inside a sealed furnace. These were dipped in a known amount of PCM, and the furnace was flushed with ultra-high purity (99.999 %) argon for a period of 0.5 hours. Thereafter, the furnace was programmed to attain a temperature of 700 °C. Although ultra-high grade purity inert gasses were used, these gasses possess some residual oxygen impurities that might have an impact on the experimental results. Hence, aluminum was used as a getter to remove any traces of oxygen (Figure 2).

3.7.3 Preparation of Substrate

Low carbon steel samples were used for the testing. These square coupons were 1/16th of an inch thick with a side length of 1 inch. The samples were sanded and washed with soap water

and then, acetone. Thereafter, these samples were sandblasted and cleaned with trichloroethylene to ensure complete removal of impurities as well as grit that might have accumulated on the sample during the sanding process. Brushes were used for the application of the coatings. Sealmet samples were coated with two coats and each coat was cured.

3.8 Results and Discussion

The results of the testing were based on the final appearance of the sample and weight change. The samples were visually checked for cracks in the coating and were subsequently weighed to deduce the performance of the respective coatings. Photographs of the samples were taken during the course of the experiments to record observations of the aforementioned factors.

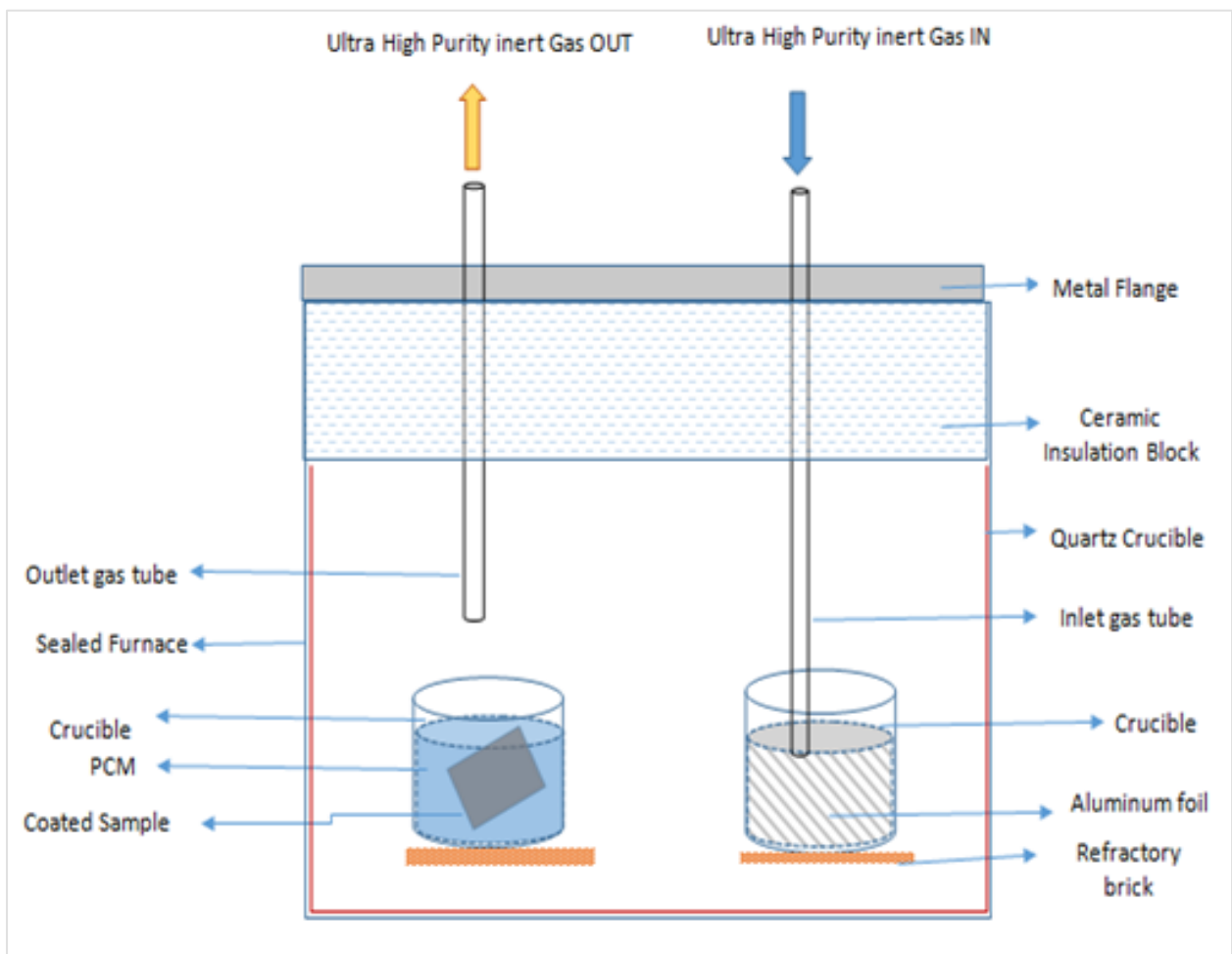


Figure 2 Cross section of the experimental setup for anaerobic testing

3.8.1 Testing in Air at 700 °C for 24-hours

1) Sealmet

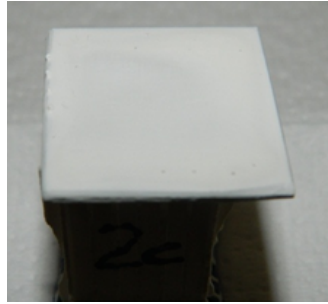
Sealmet is a water-based exterior coating manufactured by ZYP Coatings, Inc. For the preparation of these samples, the square coupon was coated twice. In order to ensure an effective coat, each coat was cured in vacuum so as to reduce chances of oxidation of the substrate during the curing process. Figure 3 depicts the sample before and after testing in air at 700 °C for 24 hours. The coating cracked and hence, this sample failed the test. The coating had issues with regards to porosity and adherence to steel substrates.



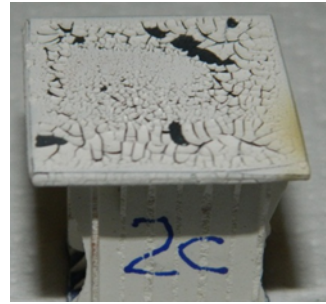
Figure 3 Sealmet sample: (a) Before testing; (b) After testing: cracks observed

2) Aremco: Pyro-paint 634-ZO

While the sample cured in air without cracking, further curing as per product instructions, led to cracking of the coating at temperatures of 95 °C. In addition, curing under vacuum was pursued to ascertain the curing results. However, the coating still scaled as shown in Figure 4. As a result, further testing of this product was not pursued.



(a)



(b)

Figure 4 Aremco paint 634ZO (a) After air dry; (b) After curing in furnace

3) Sodium silicate

Sodium silicate was also considered for testing. While temperatures of approximately 1040 °C were required for curing, the sample did not show good results. Despite various attempts, the cured sample was not uniformly coated, and bubbling in certain areas was observed. Moreover, changes in curing rates did not yield any improvements. Further testing of sodium silicate on carbon steel was not pursued.

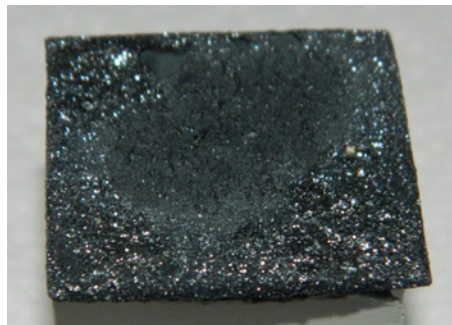


Figure 5 Bubbling observed in cured sodium silicate sample

4) Alumina adhesive

Alumina adhesive was also considered for testing. The figure below depicts the coated samples before and after testing. As can be seen, the coating chipped off along the edges of the sample. This failure could be attributed to differences in the coefficients of expansion between

the coating and substrate. Moreover, porosity of the alumina coating could also be a potential reason for descaling of the coating. Oxidation of the underlying substrate could lead to descaling of the coating on account of reduced adhesion between the oxide layer and the coating. Further experiments were also carried out employing silica in alumina adhesive to address porosity concerns as mentioned in subsequent sample testing.

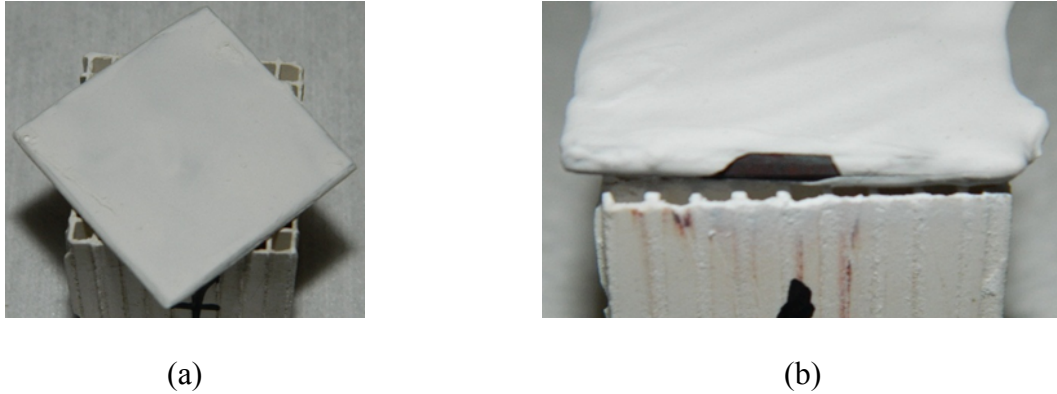


Figure 6 Alumina adhesive sample (a) Before testing; (b) After testing: chipped

5) Alumina adhesive + silica

To address the concern of adhesion of the alumina coating to the substrate, approximately 20 weight percent of silica was added to the alumina adhesive. The results are presented in the following figure.



Figure 7 Alumina adhesive + silica: (a) Before testing; (b) After testing: crack

While the alumina adhesive + silica coating failed on account of cracking, the crack was much finer as compared to the chipping observed in the case of the alumina adhesive.

6) Sealmat + sodium silicate

Application of sodium silicate on a sample coated with Sealmat was tested. The proposed hypothesis was that the use of sodium silicate would help address concerns regarding porosity of Sealmat. Prior testing had shown that Sealmat was porous to air on curing under both, aerobic and anaerobic conditions. In the current testing, the curing of sodium silicate proved to be unsuccessful as the coating scaled off as shown in Figure 8.

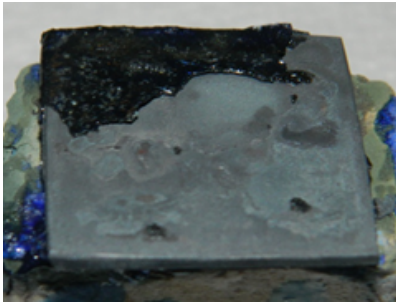


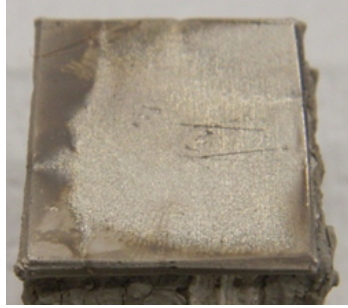
Figure 8 Scaling observed in case of Sealmat + sodium silicate coating

7) Aremco: Pyro-paint 634-ZO + sodium silicate

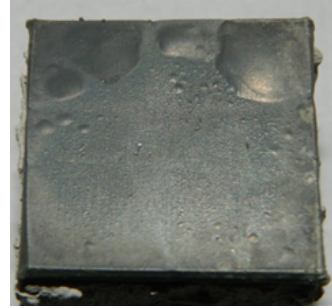
Since coating of the Aremco: Pyro-paint 634-ZO itself was unsuccessful, this testing was not pursued.

8) Electroplated nickel

Electroplated nickel (1.4 g) was tested. This electroplating was conducted in the laboratory. While the sample showed some bubbling, there was no change in the weight of the sample. Moreover, no scaling or oxidation of the substrate was detected. As a result, this sample passed the test.



(a)



(b)

Figure 9 Electroplated nickel: (a) Before testing; (b) After testing

9) Alumina adhesive + sodium silicate

In order to address the concerns regarding porosity of the alumina adhesive, coating of sodium silicate was applied on the cured alumina adhesive. Figure 10 shows the sample after the curing of sodium silicate. As can be seen, the coating was a failure on account of scaling.

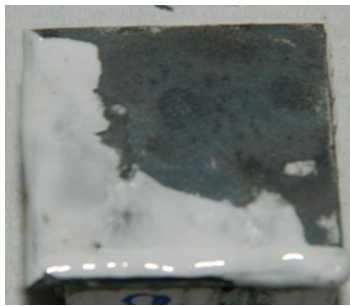


Figure 10 Alumina adhesive + sodium silicate sample failure during curing

10) Alumina adhesive + silica + sodium silicate

Sodium silicate on silica enhanced alumina adhesive coating was tested. This was done to address the porosity concerns of the adhesive. The prior results obtained with silica-enhanced alumina were better than pure alumina, however, they failed at the edges. It was hypothesized that the use of sodium silicate as a topcoat might help reduce the porosity of the coating and provide an impervious coat. This sample failed the test. The coating cracked at several locations.



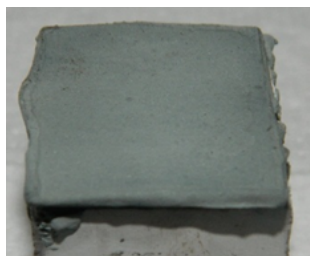
Figure 11 Alumina adhesive + silica + sodium silicate sample failure during curing

3.8.2 Testing in Anaerobic Conditions at 700 °C for 24-hours

For testing under anaerobic conditions, the samples tested were Sealmet, alumina adhesive, alumina adhesive + silica and electroplated nickel. Samples comprising sodium silicate and Aremco: Pyro-paint 634-ZO were not considered due to their unsuccessful curing.

1) Sealmet

The samples were prepared in a manner similar to the samples preparation of the aerobic testing. Figure 12 depicts the sample before and after testing in anaerobic conditions at 700 °C for 24 hours. As depicted in Figure 12, the coating scaled off and hence, was considered failed.



(a)



(b)

Figure 12 Sealmet sample (a) Before testing; (b) After testing

2) Alumina adhesive

Alumina adhesive coated samples were also tested. Figure 13 shows the crack that led to the failure of the coating. The results for the alumina adhesive coating under anaerobic conditions were slightly better than the testing conducted in aerobic conditions.

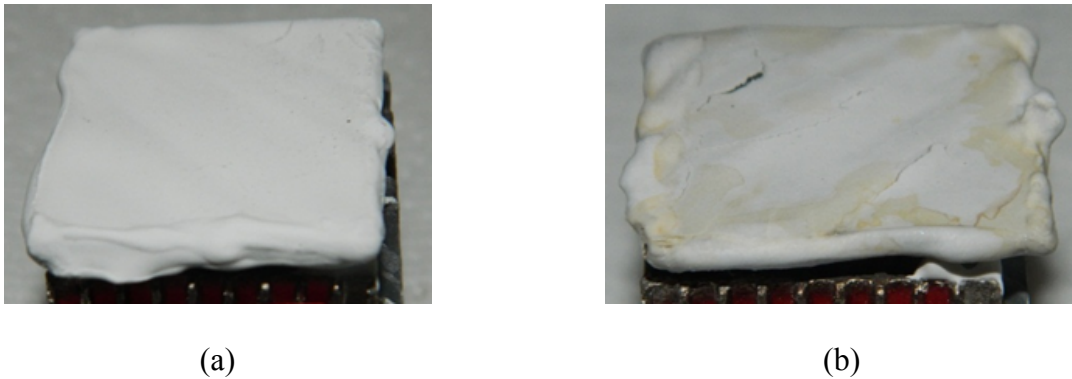


Figure 13 Alumina adhesive sample (a) Before testing; (b) After testing

3) Alumina adhesive + silica

Silica enhanced alumina adhesive was also tested for its corrosion protection capabilities in anaerobic conditions. As can be seen in Figure 14, the coating failed on account of scaling at the edges.

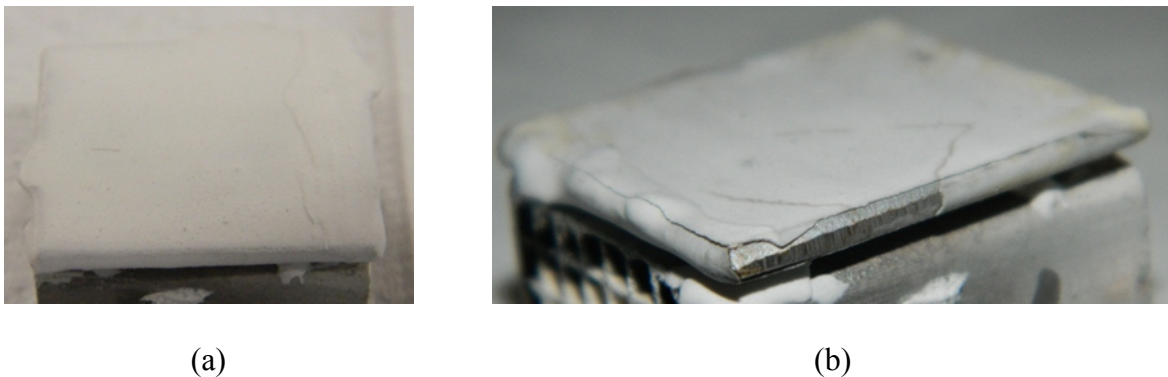


Figure 14 Alumina adhesive + silica sample (a) Before testing; (b) After testing

4) Electroplated nickel

Electroplated nickel samples were also tested under anaerobic conditions. The sample was electroplated in the laboratory with approximately 1.3 grams of nickel. The sample passed the test with approximately no weight change. The sample weighed 9.7 grams. Figure 15 shows the sample before and after testing.



Figure 15 Electroplated nickel sample (a) Before testing; (b) After testing

3.9 Optimization of Nickel Coating

Electroplated nickel samples were successful in the preliminary corrosion testing in both aerobic and anaerobic conditions. While Sealmet and alumina adhesive samples seemed promising, both coatings presented concerns with regards to porosity and adhesion to the substrate. Hence, electroplated nickel was used for corrosion protection of the exterior of the encapsulation. Optimization studies were conducted to determine the exact thickness of nickel required to protect the steel. For the interior of the encapsulation, no coating was employed on account of cost consideration and the fact that the interior of the cylinder did not contain any oxygen. The significance of the presence of oxygen or moisture towards corrosion at elevated temperatures in the presence of alkali chlorides has been discussed in chapter 2. The following section would present the results of the testing pursued for optimization of nickel thickness. In

addition to testing the optimal thickness of the coating, surface preparation of the substrate was also analyzed. This was primarily focused on the sandblasting step of the substrate preparation process.

3.10 Testing and Results

The testing of samples was conducted for approximately 336 hours in air at 700 °C. Figure 16 shows an electroplated sample before testing. The samples were both sandblasted and non-sandblasted as well as of varying thicknesses. The thicknesses of nickel evaluated were of 50 µm, 100 µm and 150 µm. These samples were similar in initial appearance.

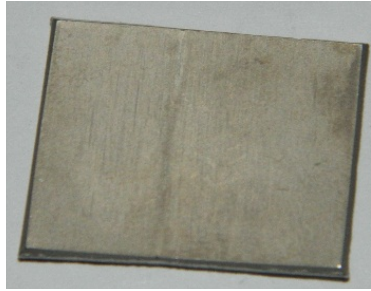
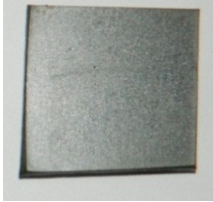
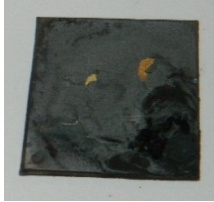


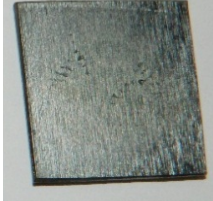

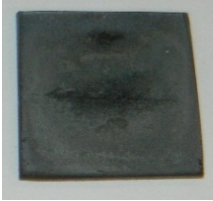



Figure 16 Electroplated sample before testing

1) 50 µm Samples

As can be seen in Table 1, testing post 48 hours shows considerable degradation for the sandblasted sample. After 336 hours of testing, there was a 2.3% weight change for the sandblasted sample since 48 hours of testing. On the other hand, the weight change for the non-sandblasted sample was approximately 0.4%. Even though the non-sandblasted sample showed better performance, both coatings failed on account of scaling. It was hypothesized that sandblasting creates small ridges on the surface thereby increasing surface roughness and reducing the quality of the nickel coating.

Table 1 Testing results for nickel coating thickness of 50 μm

Sample: Coating thickness 50 μm	After 48 hours	After 144 hours	After 240 hours	After 336 hours
Sandblasted				
Non-sandblasted				

2) 100 μm Samples

Since 48 hours of testing, the sandblasted sample depicted a weight loss of approximately 0.37%. The non-sandblasted sample showed a weight loss of 0.19%. This could be attributed to equipment error. No scaling or cracking was observed for the non-sandblasted sample. Hence, the non-sandblasted sample showed a better performance with little weight change. Table 2 depicts the samples during the course of testing.

Table 2 Testing results for nickel coating thickness of 100 μm

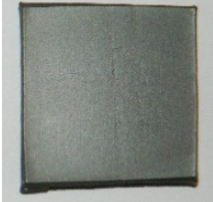
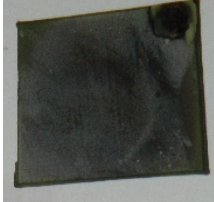

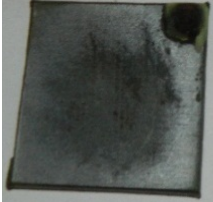
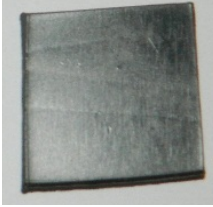


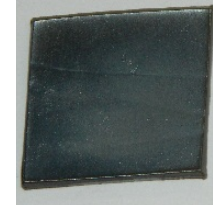
Sample: Coating thickness 100 μm	After 48 hours	After 144 hours	After 240 hours	After 336 hours
Sandblasted				


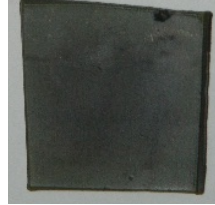

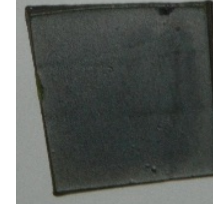
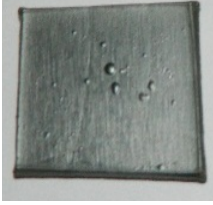



Table 2 (Continued)

Non-sandblasted				
------------------------	-----------------------------------------------------------------------------------	-----------------------------------------------------------------------------------	------------------------------------------------------------------------------------	-------------------------------------------------------------------------------------

3) 150 μm Samples

Table 3 shows the progress of the samples coated with a nickel thickness of 150 μm . In this case, considerable bubbling was observed for the non-sandblasted sample. This could be an artifact of the electroplating process. In terms of weight change, the sandblasted sample showed a change of approximately 0.15% since 48 hours of testing. On the other hand, the non-sandblasted sample showed a weight change of 0.19% during the same time period. Both samples did not show any cracking or scaling.

Table 3 Testing results for nickel coating thickness of 150 μm

Sample: Coating thickness 150 μm	After 48 hours	After 144 hours	After 240 hours	After 336 hours
Sandblasted				
Non-sandblasted				

3.11 Encapsulation Experiment

The testing results favored the 100 μm and the 150 μm nickel-plated samples that did not undergo the sandblasting process. All of these samples presented weight loss of less than 1% over the mentioned time period of 336 hours with no scaling or visible cracking. Further experimentation was carried out on sealed cylinders coated with aforementioned thicknesses of nickel to determine the best coating to employ in practical thermal energy storage applications. These encapsulations were in the form of sealed cylinders filled with PCM. This section presents the results of the aforementioned experimentation.

3.11.1 Encapsulation Lining: Corrosion Protection

Testing was carried out to observe the corrosion protection capabilities of electroplated nickel on a PCM encapsulation that used NaCl-KCl eutectic as the PCM with a melting point of 656.7 $^{\circ}\text{C}$. In order to evaluate the capabilities of electroplated nickel, two low-carbon steel cylinders were prepared in the laboratory, each containing 130 grams of NaCl-KCl eutectic as PCM. However, while one was electroplated with nickel in the laboratory having a thickness of 100 μm , the company, ADTEC, electroplated the other. The latter had a nickel thickness of approximately 150 μm .

These cylinders were thermal cycled for testing under aerobic conditions in a temperature range of 580 $^{\circ}\text{C}$ to 680 $^{\circ}\text{C}$. The weights of the cylinders were recorded and photographs were taken during various stages of the experiment. The results were inferred based on the weight change of the cylinder as well as on visual evaluation of the exterior of the sample (for cracking and scaling). The following section discusses the preparation of the cylinders and subsequent testing thereafter.

3.11.2 Preparation of Cylinders

Preparation of the cylinders was done in two steps. Firstly, the cylinders were filled with a known amount of PCM (130 grams) and sealed by welding under inert conditions in a tube furnace as shown in Figure 1. This sealing procedure has been discussed in section 3.5 of this manuscript.

Secondly, the cylinder was electroplated with 100 μm of Ni (based on prior results) in the laboratory as depicted in Figure 17. The cylinder was electroplated using three uniformly placed anodes. This was done in order to ensure a uniform thickness of the coating on the cylinder. Figure 18 shows the prepared cylinder electroplated with 100 μm of nickel.

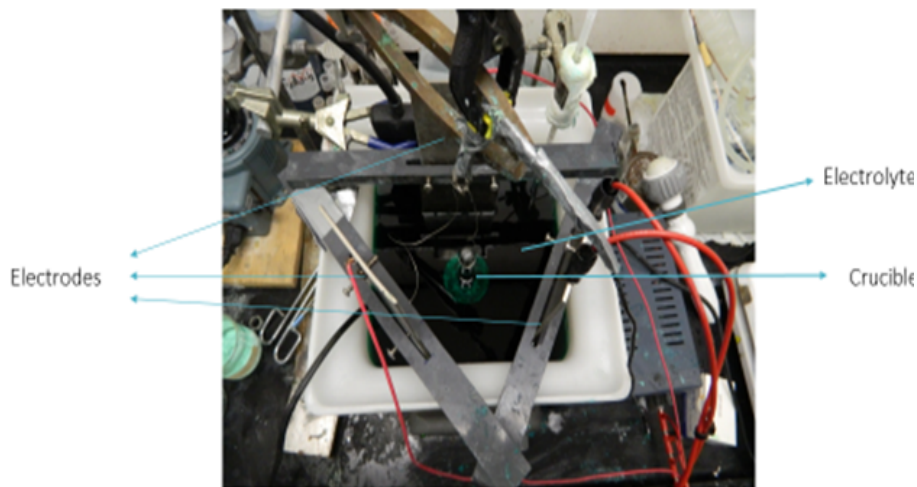


Figure 17 Electroplating apparatus



Figure 18 Electroplated cylinder

3.11.3 Testing

The cylinders were continuously exposed to air at 700 $^{\circ}\text{C}$ and visually evaluated for any surface degradation (cracking/ scaling). Afterwards, these were tested for thermal cycling in a muffle furnace under aerobic conditions. The cycle was programmed to heat the cylinder to 680 $^{\circ}\text{C}$ and maintain the temperature for a period of 2 hours. This period was preceded and succeeded by an hour each at 580 $^{\circ}\text{C}$. The weights of the cylinder were recorded after each

testing cycle in order to deduce any weight loss/gain due to oxidation/scaling. This approach to testing ensured that the encapsulated PCM underwent melting and solidification similar to practical thermal energy storage systems deployed in various practical applications.

3.11.4 Results and Discussion

The results of the testing were deduced on the basis of final appearance of the cylinder and weight change during the course of testing.

1) Cylinder electroplated in laboratory

This cylinder was first exposed to air at 680 °C for a period of two hours. Subsequently, it was setup for thermal cycling. While the cylinder showed no significant weight change in the initial testing, it failed after 20 cycles during thermal cycling as shown.



Figure 19 Cylinder electroplated in lab: After 20 cycles

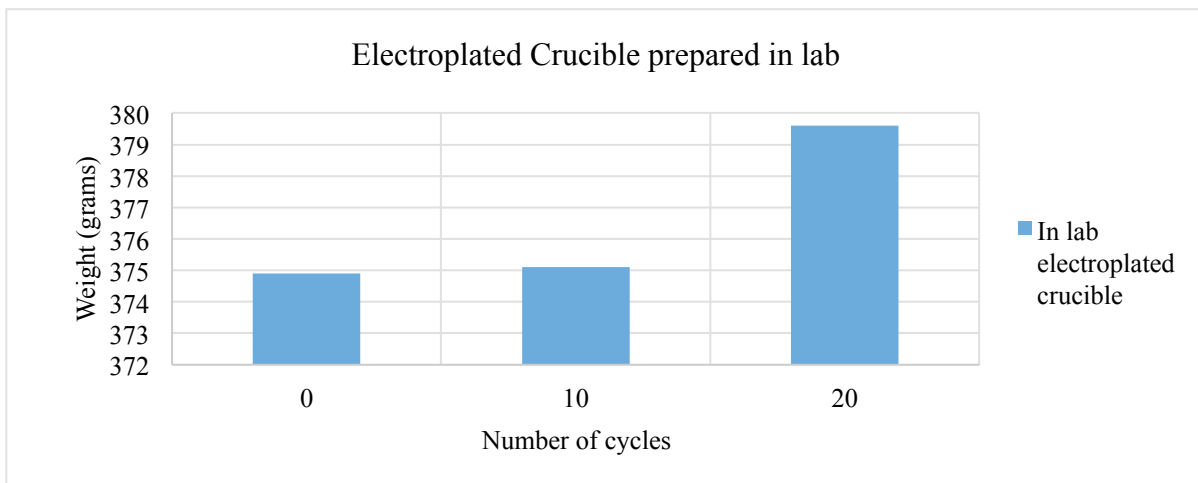


Figure 20 Weight gain of electroplated cylinder prepared in lab

2) ADTEC cylinder

The cylinder as received from ADTEC contained pinholes near the top half that were a concern regarding the corrosion protection capability of the coating. Hence, the top half was once again electroplated at the lab and the points for concern were painted for added protection.

This cylinder was first tested for continuous exposure to air at 700 °C in a muffle furnace for a total duration of 238 hours. Figure 21 depicts its weight change at various intervals during the test. The initial weight of the cylinder was 410.3 grams. After 238 hours in air, the final weight of the cylinder was 411.1 grams showing a weight gain of 0.8 grams (0.19 %).

After the initial testing, the cylinder was tested for thermal cycling. The data from thermal cycling tests is presented in Figure 23. While there was no significant weight change for the cylinder, there appeared to be a weight loss between 80 and 100 thermal cycles. Visual inspection showed no cracking/ scaling of the cylinder. Hence, this weight loss could be attributed to experimental error.

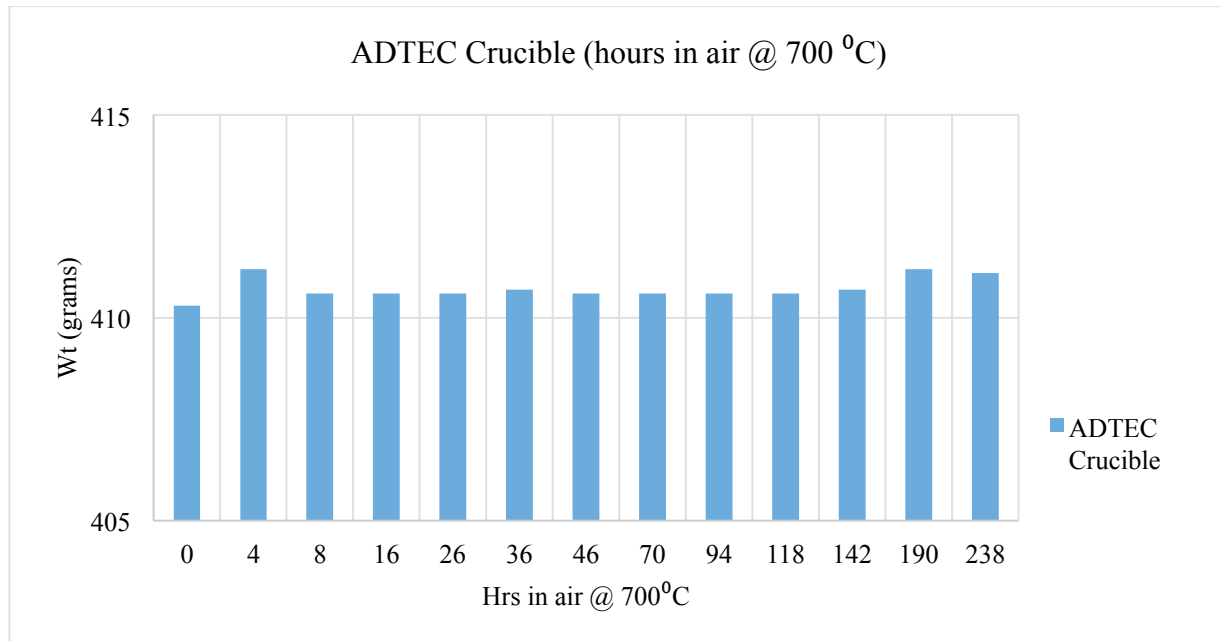


Figure 21 Weight change of ADTEC cylinder after 238 hours in air at 700 °C

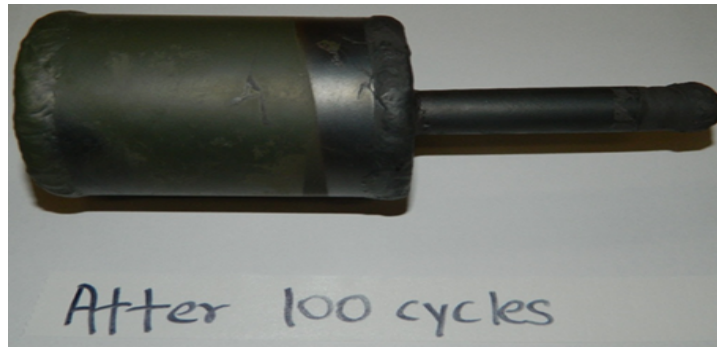


Figure 22 ADTEC cylinder after 100 thermal cycles

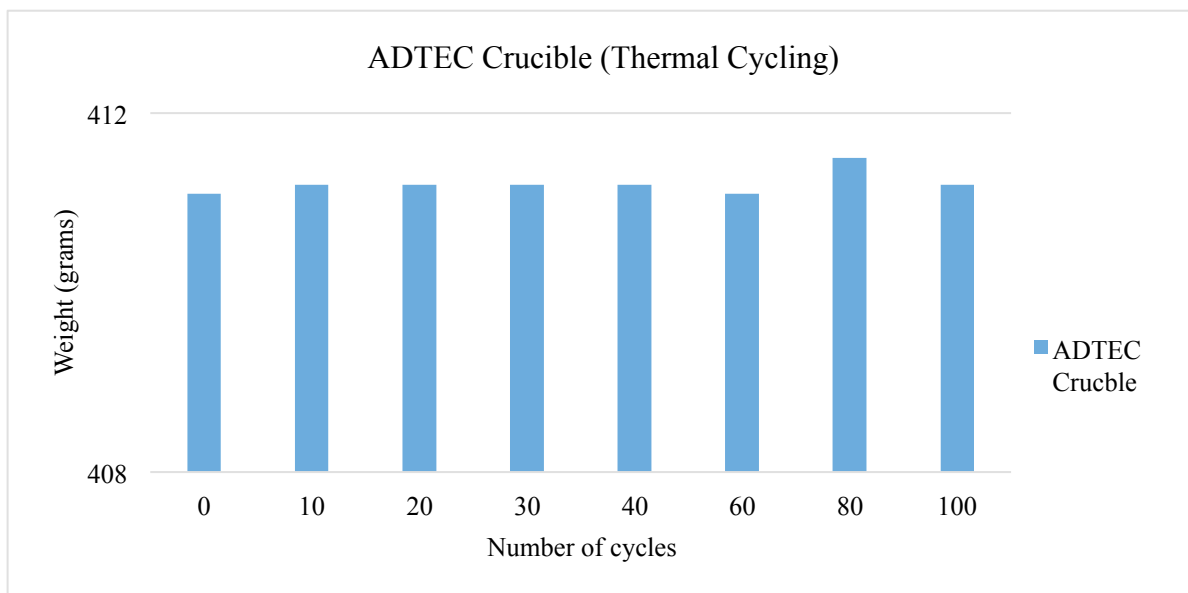


Figure 23 Weight change of ADTEC cylinder after 100 thermal cycles

Figure 22 presents the cylinder after 100 thermal cycles. The ADTEC cylinder showed a maximum weight change of 0.4 grams during the course of thermal cycling, which equates to 0.097%.

While the cylinder electroplated in lab failed the test, the ADTEC cylinder successfully passed 238 hours of continuous exposure to air at 700 °C. Furthermore, it passed 100 (2hrs @ 680 °C during each cycle) thermal cycles. This amounted to a total exposure of 438 hours of exposure to temperatures of 680 °C in air.

The results for these tests favored the 150 μm plated cylinder from ADTEC. These results justified the preparation of additional thermal energy storage cylinders with a protective coating of 150 μm nickel.

3.12 Further Testing: 150 μm Nickel-Plated Cylinder

This section presents results of further testing pursued for this cylinder, as well as other nickel-plated cylinders prepared for testing. The ADTEC cylinder was thermally cycled in aerobic conditions over a temperature range of 580 $^{\circ}\text{C}$ to 680 $^{\circ}\text{C}$ to ascertain the corrosion protection capabilities of electroplated nickel. The thermal cycle was programmed to maintain the temperature of 680 $^{\circ}\text{C}$ for a period of 2 hours as shown in Figure 24. The weights of the sealed cylinder were recorded during the course of the cycling. Additionally, photographs were taken during various stages of the experiment. Conclusions were drawn based on the weight change of the sealed cylinder as well as on evaluating the appearance of the sample (for cracking and scaling).

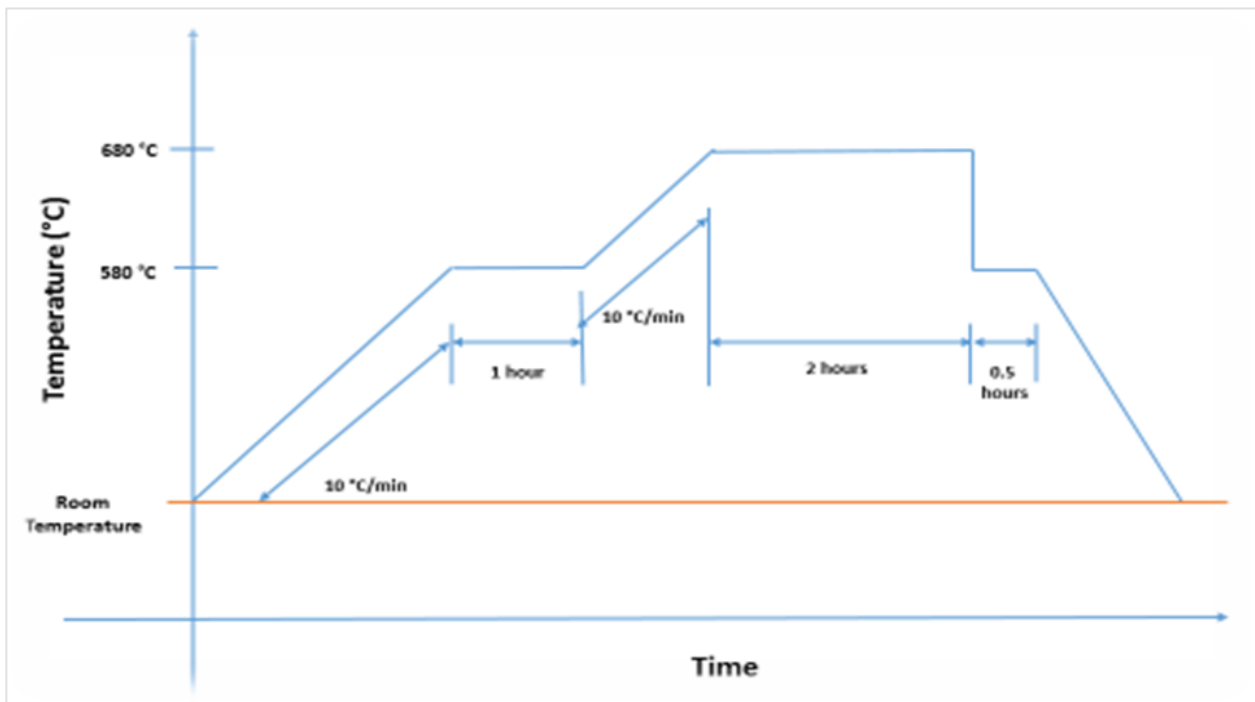


Figure 24 Thermal cycling graph (for one cycle)

3.12.1 Results: After 500 Thermal Cycles

The sealed cylinder had survived 238 hours of continuous exposure to air at 700 °C in a muffle furnace. The initial weight of the cylinder was 410.3 grams. After 238 hours of testing, a weight gain of 0.8 grams or 0.19% was observed. The weight gain was due to the conversion of nickel to an impervious layer of nickel oxide. This impervious oxide layer protected the underlying carbon steel layer.

On conclusion of this testing, the sealed cylinder was thermally cycled in a temperature range of 580 °C to 680 °C under aerobic conditions. The results of weight change for 500 thermal cycles have been presented in the figure below.

Figure 25 shows the weight change of the sealed cylinder after 500 thermal cycles. This sealed cylinder showed a maximum weight change of 0.4 grams during the course of thermal cycling, which equates to 0.097%.

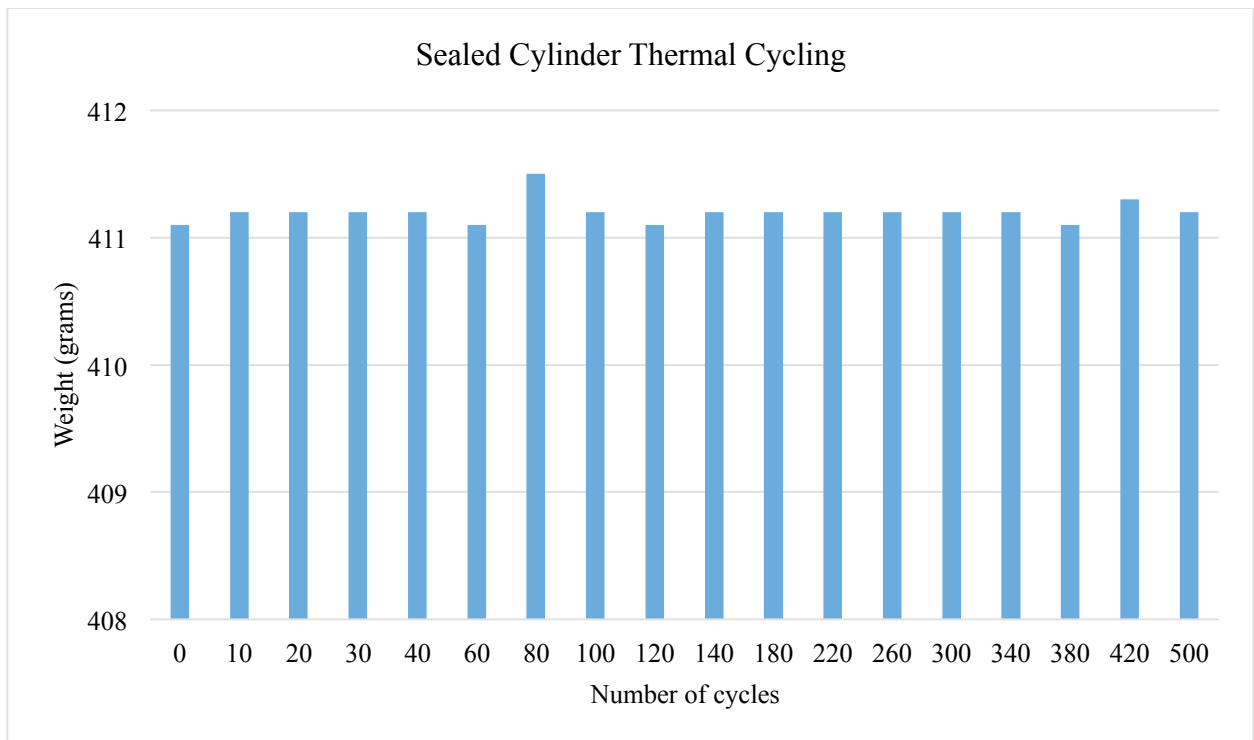


Figure 25 Weight change of sealed cylinder after 500 thermal cycles

Figure 26 depicts the sealed cylinder after 500 cycles in aerobic conditions. The sealed cylinder had successfully survived, 500 thermal cycles at a maximum temperature of 680 °C in addition to 238 hours in air at 700 °C. No leakage of PCM was observed.

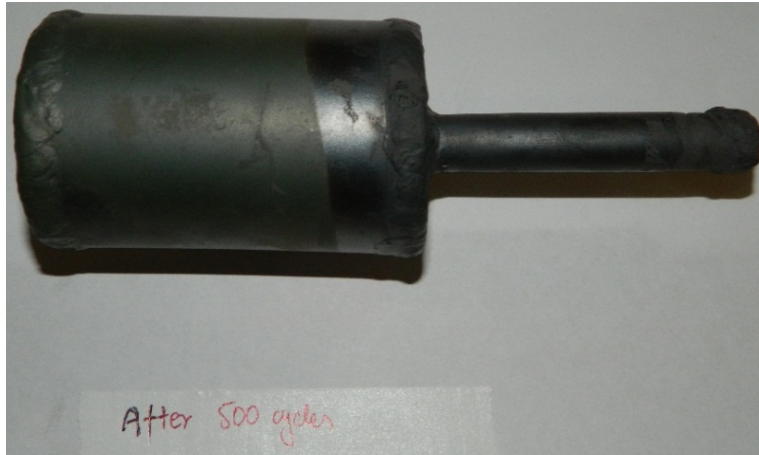


Figure 26 Sealed cylinder after 500 cycles in aerobic conditions

3.12.2 Results: After 1000 Thermal Cycles

This section presents the results for the thermal cycling of the sealed cylinder after 1000 thermal cycles. Up till now it had successfully passed 500 thermal cycles in addition to 238 hours in air at temperature of 700 °C with a weight change of less than 1%.

Figure 27 presents results of weight change of the sealed cylinder during the course of 1000 thermal cycles. Performance of the cylinder was evaluated by monitoring the change in the weight of the cylinder and observing the exterior surface for any physical degradation (cracking and scaling). The observations were documented by taking photographs at various stages of the experiment.

The cylinder had successfully passed 1000 thermal cycles, i.e., no leakage of PCM was observed and no significant degradation of the exterior nickel coating was detected.

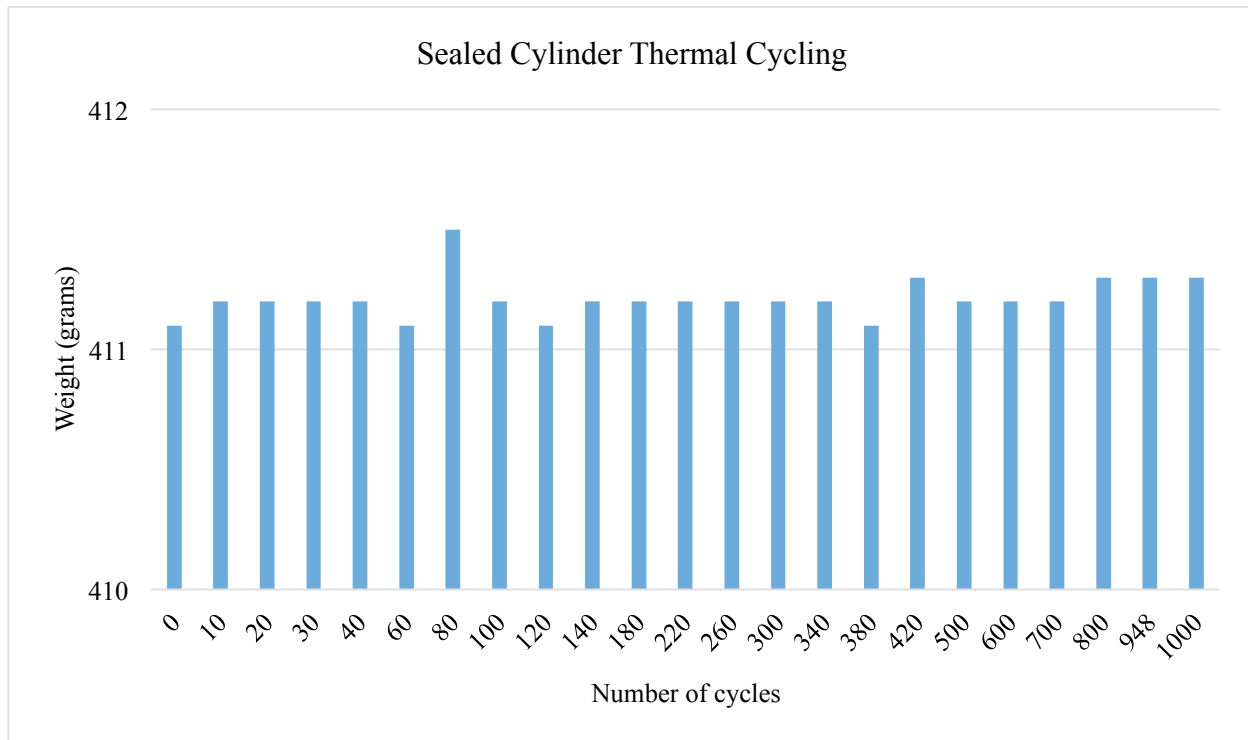


Figure 27 Weight change of sealed cylinder after 1000 thermal cycles



Figure 28 Sealed cylinder after 1000 cycles in aerobic conditions

The initial weight of the sample was 410.3 g. After 1000 thermal cycles, it increased by 1.0 g (0.24%). No significant change in the weight of the cylinder was noticed after 800 thermal cycles.

3.12.3 Results: After 1700 Thermal Cycles

As in prior cases, weight of the cylinder and photographs of the sample were recorded during the course of thermal cycling. Moreover, two additional cylinders were prepared that employed nickel and chrome for protection from corrosion.

Figure 29 presents the weight change of the samples during the course of 1700 thermal cycles. As can be observed from the experimental results, no significant weight change occurred other than the experimental error discussed previously for 80 thermal cycles. Hence, based on weight change, the cylinder showed no significant degradation.

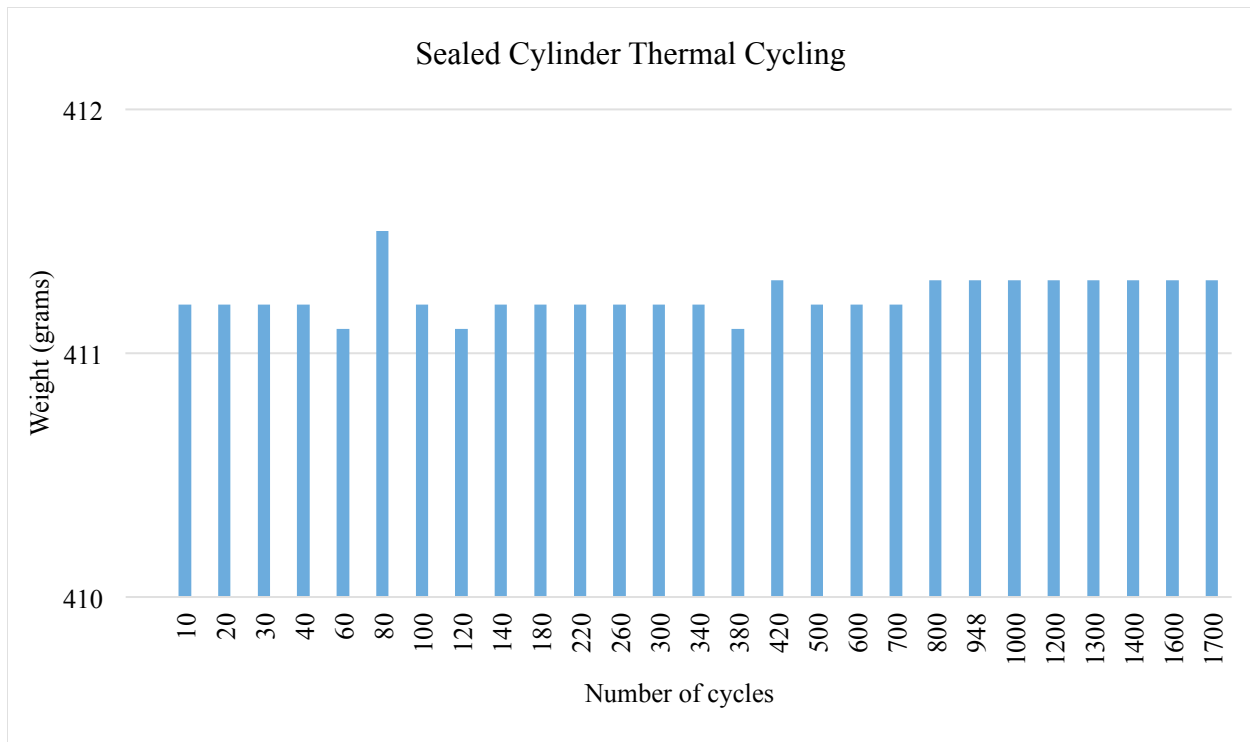


Figure 29 Weight change of sealed cylinder after 1700 thermal cycles

Figure 30 shows the sample after 1700 thermal cycles. While the sample did not show any weight change, the cylinder had bent on account of continuous thermal cycling. Further thermal cycling led to failure of the sealed cylinder as shown in Figure 31.

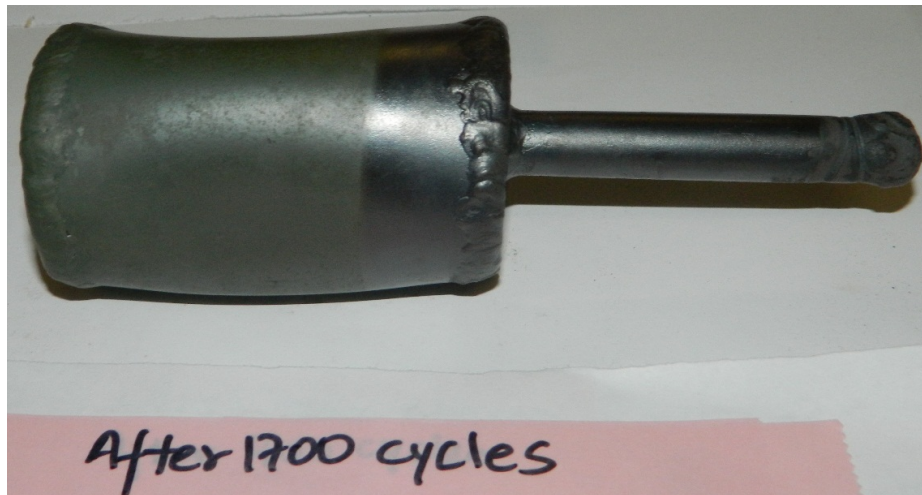


Figure 30 Sealed cylinder after 1700 cycles in aerobic conditions

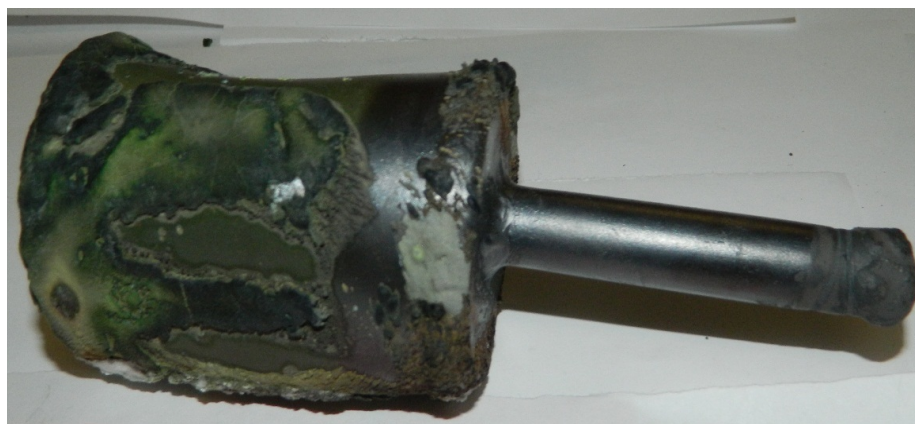


Figure 31 Failure of electroplated 150 μm Ni cylinder between 1700 and 1800 cycles

It is interesting to note that in Figure 31, even though the sample corroded on account of leakage of PCM, the nickel-plating around the fill tube was not affected. The fill tube did not show any signs of corrosion.

As can be seen from the DSC curves in Figure 32, less than 1% change in magnitude of latent heat of fusion was observed. The value changed from 321.6 J/g before cycling to 322.8 J/g after 1700 thermal cycles.

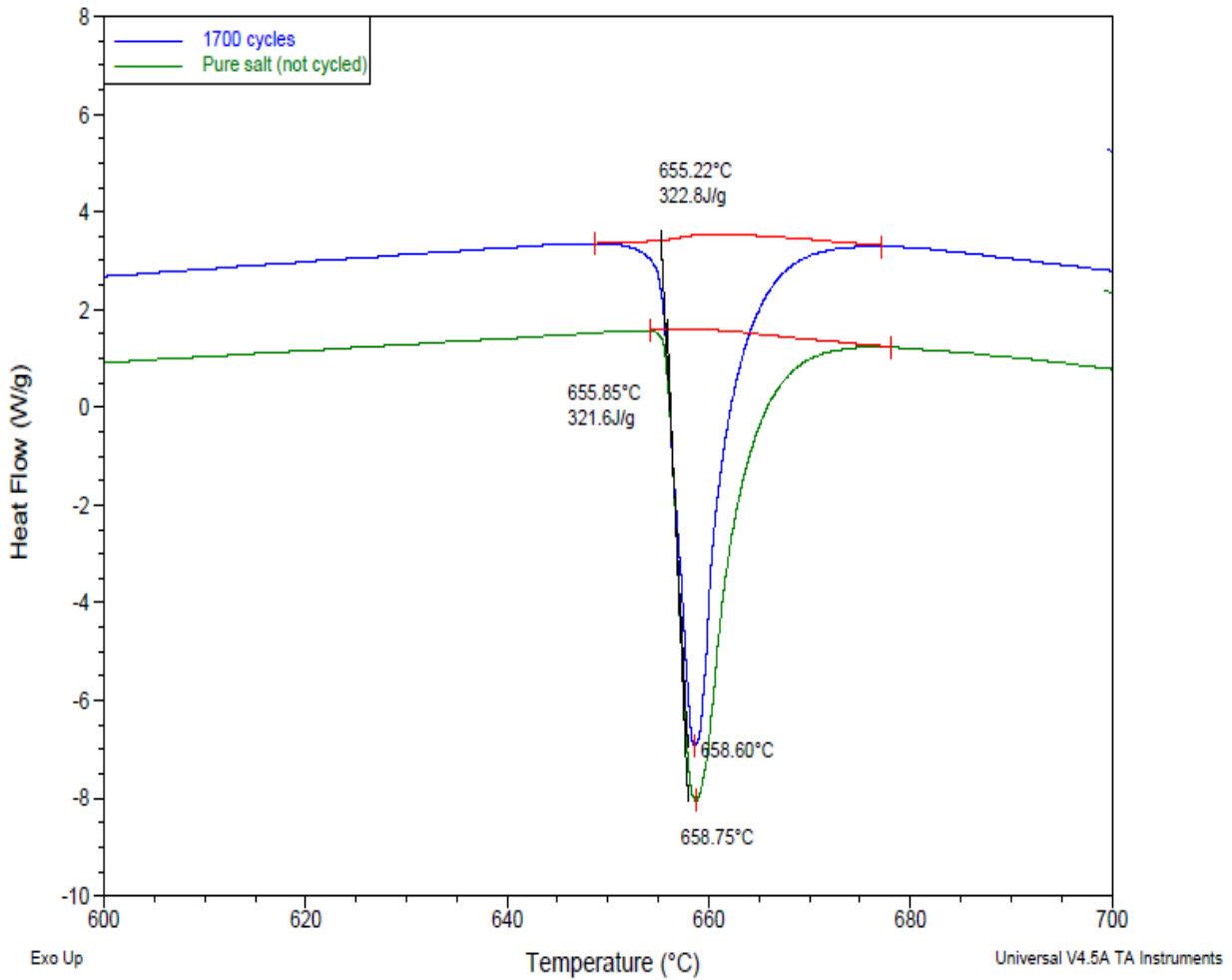


Figure 32 DSC curve of PCM before and after undergoing 1700 thermal cycles

Furthermore, two more cylinders (A & B) were prepared with 150 μm of nickel for protective coating. Both these cylinders used NaCl-KCl eutectic as the PCM. One of these cylinders (cylinder A) was subjected to thermal cycling. This sample successfully underwent 60 thermal cycles under previously discussed thermal cycling conditions. The initial weight of this sample was 391.3 g. After 60 thermal cycles, the weight of the cylinder was found to be 391.5 g. No scaling of the coating was observed as shown in Figure 33.

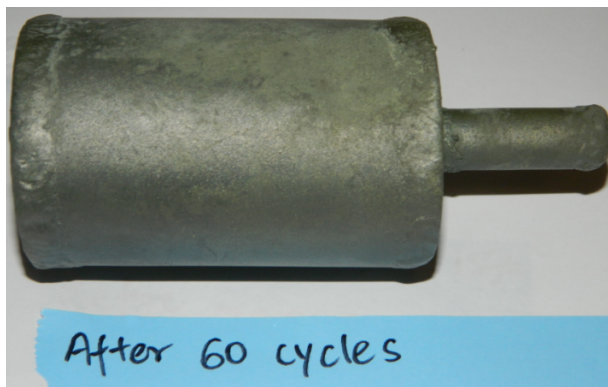


Figure 33 Electroplated Ni cylinder A (150 μm of electroplated nickel) after 60 cycles

During further testing, this cylinder A successfully underwent 200 thermal cycles under conditions discussed earlier. The initial weight of this sample was 391.3 g. After 200 thermal cycles, the weight of the cylinder was found to be 391.6 g. However, while the sample successfully passed 200 thermal cycles, it failed during the next 100 cycles of testing. Figure 34 depicts the point of failure of the failed sample after 200 cycles.



Figure 34 Electroplated Ni cylinder A (150 μm of electroplated nickel) after 200 cycles and the point of failure

The following Figure 35 displays the SEM image of one of the cylinders before thermal cycling. As can be seen, the average thickness of nickel coating was 150 μm . While the top lighter area demarcated by arrows indicates nickel, the bottom dark area represents steel. The

sample for SEM imaging were placed in epoxy molds for sample holding as displayed by the dark gray region in the top thirds of the image.

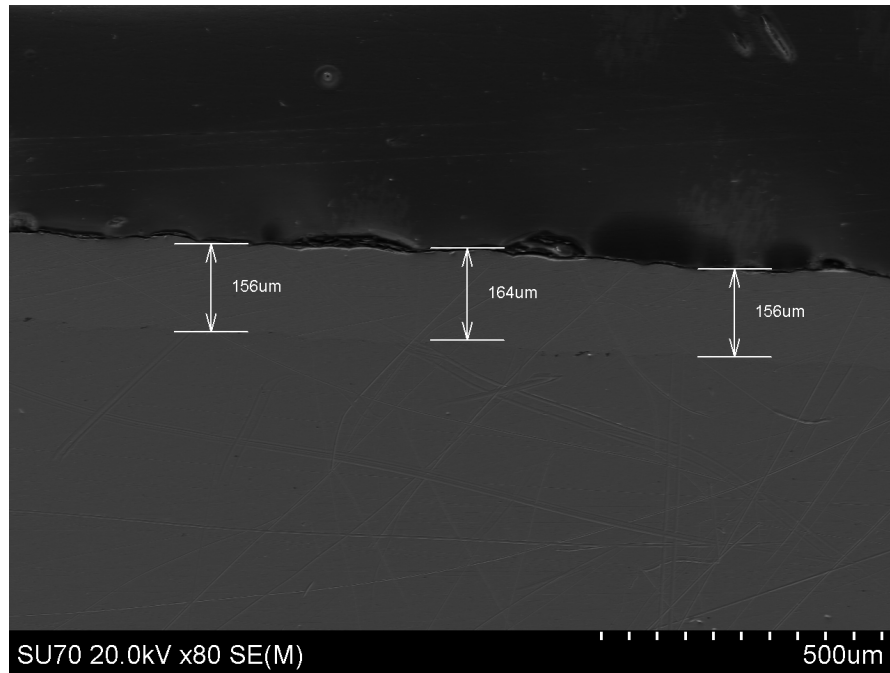


Figure 35 SEM image depicting the thickness of nickel layer for the tested cylinders

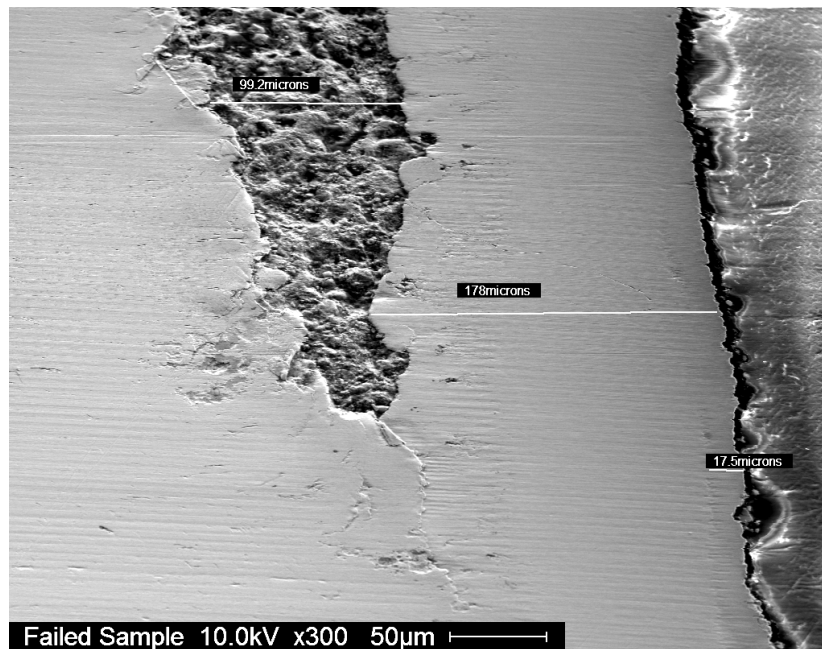


Figure 36 SEM image depicting the point of failure of cylinder A after 200 thermal cycles

As can be seen in Figure 36, the nickel oxide layer had peeled off the substrate, exposing the carbon steel and thus, led to failure.

Cylinder B, on the other hand, successfully passed the first 100 thermal cycles. However, it failed to complete 200 cycles. Figure 37 depicts the failed sample.



Figure 37 Electroplated Ni cylinder B (150 μm of electroplated nickel) after 100 cycles and the point of failure

Both of these 150 μm of nickel-plated cylinders (A and B), the points of failure were at (or very close to) the point of welding. It appears that while 150 μm of nickel has shown sufficient ability to protect the substrate from oxidation in case of flat specimens, it fails in cylindrical geometries at points of welding. Irregularities caused at these points on account of welding could lead to uneven coating and hence insufficient protection for the carbon steel substrate. More research would be required to determine optimal welding techniques or thickness of the nickel coating would have to be increased for successful encapsulation.

3.13 Chrome Coating Test

Thermal cycling tests conducted on nickel electroplated cylinders validated the encapsulation procedure of the PCMs as well as the resilience of the metallic encapsulation. However, high cost of nickel remained a concern. Hence further testing was carried out with different coating materials. Chrome was one of the materials shortlisted for thermal cycle testing.

Since prior testing showed that areas with welding proved to be points of failure during thermal cycling tests. Hence, samples of carbon steel were prepared and welded together. These samples were then coated with 150 μm of chrome. The chrome sample prepared had an initial weight of 79.396 g. It successfully passed 800 thermal cycles in a temperature range of 580 $^{\circ}\text{C}$ to 680 $^{\circ}\text{C}$ under aerobic conditions. After 800 thermal cycles its final weight was 79.562 g. This translated to a weight change of less than 1%. Moreover, no scaling of the coating was observed. This sample is undergoing further testing. Figure 38 depicts the sample before and after testing.



(a) Before thermal cycling



(b) After 800 thermal cycles

Figure 38 Chrome-plated samples (a) Before testing; (b) After testing

Based on these results, more welded carbon steel samples were prepared and coated with varying thicknesses of chrome. This was done in order to determine the optimum thickness of chrome required for protecting the carbon steel substrate. These samples had chrome thickness of

75 μm , 100 μm , 125 μm and 150 μm . The results for these samples after 200 thermal cycles have been presented in Table 4. The thermal cycling tests were conducted under the previously stated conditions.

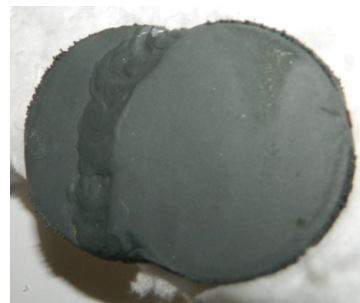
Table 4 Weight change of samples through thermal cycling

Chrome thickness	Initial weight (g)	Weight after 200 thermal cycles (g)
75 μm	62.263	62.288
100 μm	62.362	62.341
125 μm	67.563	67.638
150 μm	70.184	70.237

As seen from Table 4, all samples reported a change of weigh of less than 1%. All samples showed a weight increase after testing except for 100 μm sample. This could be on account of erroneous initial reading, as the sample did not show any significant deterioration/ scaling. Further testing lead to scaling of the coating on most samples. Hence, additional samples were sought to continue testing of chrome as protective coating for thermal cycling test of the encapsulation. Figure 39 depicts one of the samples after 200 thermal cycles.



(a) Before thermal cycling



(b) After 200 thermal cycles

Figure 39 Chrome-plated (75 μm) samples (a) Before testing; (b) After 200 cycles

In addition to these welded samples, a cylinder encapsulating NaCl-KCl eutectic as PCM was also constructed as shown in Figure 40.



Figure 40 Chrome plated cylinder before testing (150 μm)



Figure 41 Chrome-plated cylinder (150 μm) failed after 3 thermal cycles

This cylinder was plated with 150 μm of chrome and was subjected to thermal cycling tests. However, the coating on this cylinder was not of good finish. As a result, the cylinder failed after 3 thermal cycles as shown in Figure 41.

With respect to chrome, while one of the samples had survived 800 thermal cycles, more testing is required for evaluating the protection capability of the coating on cylindrical geometry of the encapsulation.

3.14 Aluminum Coating Test

In addition to chrome, aluminum is an additional contender that possesses corrosion protection capability along with cost effectiveness. Hence, preliminary testing with aluminum coated sample was also performed. Carbon steel samples namely CRCS#1 and 2 were dip coated with aluminum at a partner facility while testing was carried out in the laboratory.

While CRCS#1 was dipped in molten aluminum for 2 minutes to obtain a thin coating, CRCS#2 was dipped for 5-7 minutes. Before testing in the laboratory was carried out, these samples were already tested for 20 hours at 900 $^{\circ}\text{C}$ in air. No scaling was observed.

Figure 42 depicts the weight change of the samples during the course of the testing. The maximum weight change was observed during the first 100 hours of testing. Thereafter, there has been a small gradual increase in weight. This weight gain can be attributed to the possible conversion of aluminum to aluminum oxide. While an oxide coating had been observed, no scaling was recorded in the case of these samples. Furthermore, the oxide coating was resilient and did not flake off even on being scraped with a spatula. Therefore, further testing is recommended for these samples.

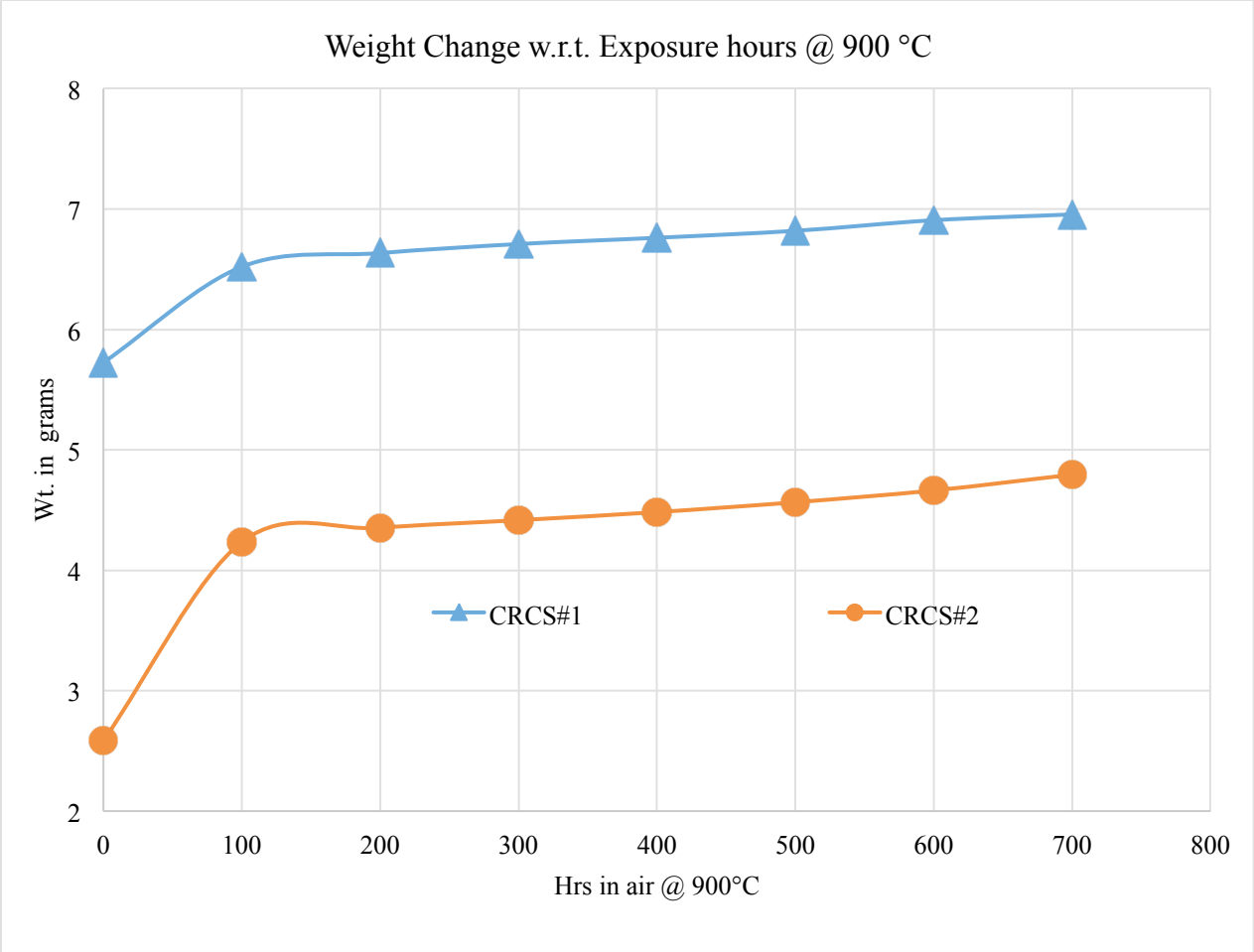


Figure 42 Weight change of aluminum coated carbon steel samples during testing in air at 900°C

CHAPTER 4: DISCUSSION AND CONCLUSION

Experimental results presented in chapter 3 had showed promise for nickel-plated encapsulations. While two samples had successfully passed 100 thermal cycles. One sample had successfully passed 1700 thermal cycles. In addition to nickel, chrome and aluminum were also tested as corrosion resistant coatings for protecting steel. The chrome-plated coupon had shown promising results. Based on these experiments, it is recommended to test additional samples of chrome-plated and nickel-plated cylinders. In the case of nickel-plated cylinders, most failures were observed along the weld joints. Since these joints present a highly uneven surface to coat, it seems plausible that these locations be the points of failure owing to improper coating. Hence, it is recommended to prepare samples that have better finish of the welded joints. Better finish would ensure a smoother surface, and, a better coating. While, nickel-plated samples are recommended for testing, the author would also recommend testing for chrome-plated cylinders. Since chrome is cheaper than nickel, a thicker coating of chrome could still prove to be more cost-effective than nickel.

In addition to chrome and nickel, the author would recommend testing aluminum coated steel for the above mentioned applications. While prior results have shown a low weight change for the aluminum coated samples over several thermal cycles, further experimentation should be carried out to test this material and determine its efficacy for the intended application.

While this research has presented results for the evaluation and optimization of corrosion resistant coating materials for steel in elevated temperature applications, further experimentation is required to collect the thermal performance characteristics of the encapsulation. Thermal

performance evaluation of these encapsulations in power plant like conditions of temperature and pressure would determine their effectiveness and hence deployment in commercial scale power plants.

This testing for thermal performance should be conducted on two scales. Firstly, it should be conducted on the individual encapsulation level. This would enable us to understand the thermal behavior of the individual thermal energy cell. This knowledge would be invaluable to determine the behavior of a large-scale system. Secondly, a pilot-scale study of the system is also required to determine the performance of the thermal energy unit as a whole. Each thermal energy unit could comprise of several thermal energy cells arranged in a packed bed. Alternately, these thermal energy cells could be deployed in a thermal energy unit in a shell and tube configuration.

Experimental data obtained from such studies would facilitate the development of computational models that accurately predict the thermal performance of the system. Development of such models would greatly increase the pace of research thereby aiding the development of optimum storage technology for thermal energy storage at elevated temperatures. Productive research in the field of thermal energy storage could help establish a more competitive solar energy sector and thus, a sustainable future.

REFERENCES

- [1] S. Izquierdo, C. Montañés, C. Dopazo and N. Fueyo, "Analysis of CSP plants for the definition of energy policies: The influence on electricity cost of solar multiples, capacity factors and energy storage," *Energy Policy*, vol. 38, no. 10, p. 6215–6221, 2010.
- [2] J. Stekli, L. Irwin and R. Pitchumani, "Technical Challenges and Opportunities for Concentrating Solar Power With Thermal Energy Storage," *J. Thermal Sci. Eng. Appl*, vol. 5, no. 2, 2013.
- [3] P. Denholm and M. Hand, "Grid flexibility and storage required to achieve very high penetration of variable renewable electricity," *Energy Policy*, vol. 39, no. 3, p. 1817–1830, 2011.
- [4] D. Y. Goswami, F. Kreith and J. F. Kreider, "Principles of Solar Engineering," Philadelphia, PA: Taylor & Francis, 2000.
- [5] A. Gil, M. Medrano, I. Martorell, A. La'zaro, P. Dolado and B. Zalba, "State of the art on high temperature thermal energy storage for power generation. Part 1—Concepts, materials and modellization," *Renewable and Sustainable Energy Reviews*, vol. 14, no. 14, pp. 31-55, 2010.
- [6] A. Abhat, "Low Temperature Latent Heat Thermal Energy Storage: Heat Storage," *Solar Energy*, vol. 10, no. 4, pp. 313-332, 1983.
- [7] G. A. Lane, "Solar heat storage: latent heat materials," Boca Baton, Fla.: CRC Press, 1983.
- [8] İ. E. Dinçer and M. A. Rosen, "Thermal energy storage: systems and applications," Hoboken, N.J.: Wiley, 2011.
- [9] B. Zalba, M. Jose', L. F. Cabeza and H. Mehling, "Review on thermal energy storage with phase change materials, heat transfer analysis and applications," *Applied Thermal Engineering*, vol. 23, no. 3, pp. 251-283, 2003.
- [10] M. Liu, W. Saman and F. Bruno, "Review on storage materials and thermal performance enhancement techniques for high temperature phase change thermal storage systems," *Renewable and Sustainable Energy Reviews*, vol. 16, no. 4, pp. 2118-2132, 2012.

- [11] R. M. Abdel-Wahed, J. W. Ramsey and E. M. Sparrow, "Photographic study of melting about an embedded horizontal heating cylinder," *International Journal of Heat and Mass Transfer*, vol. 22, no. 1, pp. 171-173, 1979.
- [12] K. Ermis, A. Ereke and I. Dincer, "Heat transfer analysis of phase change process in a finned-tube thermal energy storage system using artificial neural network," *International Journal of Heat and Mass Transfer*, vol. 50, no. 15-16, pp. 3163-3175, 2007.
- [13] F. Agyenim, P. Eames and M. Smyth, "A comparison of heat transfer enhancement in a medium temperature thermal energy storage heat exchanger using fins," *Solar Energy*, vol. 83, no. 9, pp. 1509-1520, 2009.
- [14] B. Horbaniuc, G. Dumitrascu and A. Popescu, "Mathematical models for the study of solidification within a longitudinally finned heat pipe latent heat thermal storage system," *Energy Conversion and Management*, vol. 40, no. 15-16, pp. 1765-1774, 1999.
- [15] K. Sasaguchi and H. Takeo, "Effect of the orientation of a finned surface on the melting of frozen porous media," *International Journal of Heat and Mass Transfer*, vol. 37, no. 1, pp. 13-26, 1994.
- [16] E. M. Sparrow, E. D. Larson and J. W. Ramsey, "Freezing on a finned tube for either conduction-controlled or natural-convection-controlled heat transfer," *International Journal of Heat and Mass Transfer*, vol. 24, no. 2, pp. 273-284, 1981.
- [17] Y. Zhang and A. Faghri, "Heat transfer enhancement in latent heat thermal energy storage system by using the internally finned tube," *International Journal of Heat and Mass Transfer*, vol. 39, no. 15, pp. 3165-3173, 1996.
- [18] R. Velraj, R. V. Seeniraj, B. Hafner, C. Faber and K. Schwarzer, "Experimental analysis and numerical modelling of inward solidification on a finned vertical tube for a latent heat storage unit," *Solar Energy*, vol. 60, no. 5, pp. 281-290, 1997.
- [19] K. A. Ismail, C. L. Alves and M. S. Modesto, "Numerical and experimental study on the solidification of PCM around a vertical axially finned isothermal cylinder," *Applied Thermal Engineering*, vol. 21, no. 1, pp. 53-77, 2001.
- [20] J. C. Choi and S. D. Kim, "Heat-transfer characteristics of a latent heat storage system using $\text{MgCl}_2 \cdot 6\text{H}_2\text{O}$," *Energy*, vol. 17, no. 12, pp. 1153-1164, 1992.
- [21] J. P. Trelles and J. J. Dufly, "Numerical simulation of porous latent heat thermal energy storage for thermoelectric cooling," *Applied Thermal Engineering*, vol. 23, no. 13, pp. 1647-1664, 2003.

- [22] C. J. Hoogendoorn and G. C. Bart, "Performance and modelling of latent heat stores," *Solar Energy*, vol. 48, no. 1, pp. 53-58, 1992.
- [23] E.-B. S. Mettawee and G. M. Assassa, "Thermal conductivity enhancement in a latent heat storage system," *Solar Energy*, vol. 81, no. 7, pp. 839-845, 2007.
- [24] F. Agyenim, P. Eames and M. Smyth, "Heat transfer enhancement in medium temperature thermal energy storage system using a multitube heat transfer array," *Renewable Energy*, vol. 35, no. 1, pp. 198-207, 2010.
- [25] R. Hendra, T. M. Hamdani and H. H. Masjuki, "Thermal and melting heat transfer characteristics in a latent heat storage system using mikro," *Applied Thermal Engineering*, vol. 25, no. 10, pp. 1503-1515, 2005.
- [26] J. Wang, G. Chen and H. Jiang, "Theoretical study on a novel phase change process," *International Journal of Energy Research*, vol. 23, no. 4, pp. 287-294, 1999.
- [27] J. Wang, Y. Ouyang and G. Chen, "Experimental study on charging processes of a cylindrical heat storage employing multiple-phase-change materials," *International Journal of Energy Research*, vol. 25, no. 5, pp. 439-447, 2001.
- [28] M. M. Farid and A. Kanzawa, "Thermal performance of a heat storage module using PCM's with different melting temperatures: Mathematical modeling," *Journal of Solar Energy Engineering*, vol. 111, no. 2, pp. 152-157, 1989.
- [29] P. W. Griffiths and P. C. Eames, "Performance of chilled ceiling panels using phase change material slurries as the heat transport medium," *Applied Thermal Engineering*, vol. 27, no. 10, pp. 1756-1760, 2007.
- [30] M. N. Hawlader, M. S. Uddin and M. M. Khin, "Microencapsulated PCM thermal-energy storage system," *Applied Energy*, vol. 74, no. 1-2, pp. 195-202, 2003.
- [31] A. F. Regin, S. C. Solanki and J. S. Saini, "Heat transfer characteristics of thermal energy storage system using PCM capsules: A review," *Renewable and Sustainable Energy Reviews*, vol. 12, no. 9, pp. 2438-2458, 2008.
- [32] P. B. Salunkhe and P. S. Shembekar, "A review on effect of phase change material encapsulation on the thermal performance of a system," *Renewable and Sustainable Energy Reviews*, vol. 16, no. 8, pp. 5603-5616, 2012.
- [33] A. M. Khudhair and M. M. Farid, "A review on energy conservation in building applications with thermal storage by latent heat using phase change materials," *Energy Conversion and Management*, vol. 45, no. 2, pp. 263-275, 2004.

- [34] G. Fang, H. Li, F. Yang and S. Wu, "Preparation and characterization of nano-encapsulated n-tetradecane as phase change material for thermal energy storage," *Chemical Engineering Journal*, vol. 153, no. 1-3, pp. 217-221, 2009.
- [35] Y. Fang, S. Kuang, X. Gao and Z. Zhang, "Preparation and characterization of novel nanoencapsulated phase change materials," *Energy Conversion and Management*, vol. 49, no. 12, pp. 3704-3707, 2008.
- [36] N. Hiramatsu, Y. Uematsu, T. Tanaka and M. Kinugasa, "Effects of alloying elements on NaCl-induced hot corrosion of stainless steels," *Materials Science and Engineering*, vol. 120-121, no. 1, pp. 319-328, 1989.
- [37] C. A. Sequeira and M. G. Hocking, "Hot Corrosion of Nimonic 105 in Sodium Sulfate-Sodium Chloride Melts," *Corrosion*, vol. 37, no. 7, pp. 392-407, 1981.
- [38] J. Lehmusto, P. Yrjas, B. J. Skrifvars and M. Hupa, "High temperature corrosion of superheater steels by KCl and K₂CO₃ under dry and wet conditions," *Fuel Processing Technology*, vol. 104, pp. 253-264, 2012.
- [39] K. Vignarooban, P. Pugazhendhi, C. Tucker, D. Gervasio and M. Kannan, "Corrosion resistance of Hastelloys in molten metal-chloride heat-transfer fluids for concentrating solar power applications," *Solar Energy*, vol. 103, p. 62-69, 2014.
- [40] Y. Zhou, J. Chen, X. Yang and Z. Liu, "Effects of Cr, Ni and Cu on the Corrosion Behavior of Low Carbon Microalloying Steel in a Cl⁻ Containing Environment," *Journal of Materials Science & Technology*, vol. 29, no. 2, pp. 168-174, 2013.
- [41] R. T. Coyle, T. M. Thomas and G. Y. Lai, "Exploratory corrosion tests on alloys in molten salts at 900 °C," *Journal of Materials for Energy Systems*, vol. 7, no. 4, pp. 345-352, 1986.
- [42] H. E. Evans, D. Hilton and R. Holm, "Chromium-depleted zones and the oxidation process in stainless steels," *Oxidation of Metals*, vol. 10, no. 3, pp. 149-161, 1976.
- [43] B. P. Mohanty and D. Shores, "Role of chlorides in hot corrosion of a cast Fe-Cr-Ni alloy. Part I: Experimental studies," *Corrosion Science*, vol. 46, pp. 2893-2907, 2004.
- [44] R. Shankar and U. A. Kamachi Mudali, "Corrosion of type 316L stainless steel in molten LiCl-KCl salt," *Materials and Corrosion*, vol. 59, no. 11, pp. 878-882, 2008.
- [45] M. A. Uusitalo, P. M. Vuoristo and T. A. Mäntylä, "High temperature corrosion of coatings and boiler steels below chlorine-containing salt deposits," *Corrosion Science*, vol. 46, no. 6, pp. 1311-1331, 2004.

- [46] B. N. Mordyuk, G. I. Prokopenko, M. Vasylyev and M. O. Iefimov, "Effect of structure evolution induced by ultrasonic peening on the corrosion behavior of AISI-321 stainless steel," *Materials Science and Engineering A*, vol. 458, pp. 253-261, 2007.
- [47] K. Kwong, A. Petty, J. Bennett, R. Krabbe and H. Thomas, "Wear mechanisms of chromia refractories in slagging gasifiers," *International Journal of Applied Ceramic Technology*, vol. 4, pp. 503-513, 2007.
- [48] J. Szargut, D. Morris and F. Steward, "Exergy analysis of thermal, chemical, and metallurgical processes," Hemisphere Publishing, New York, NY, 1987.
- [49] D. o. E. U.S., "SunShot Vision Study. U.S. Department of Energy," U.S. Department of Energy. NREL Report No. BK5200-47927; DOE/GO-102012-3037, 2012.